

Chapter-6

Development of molecular fluorophore for sensing thorium ion

6.1 Introduction

Wide applications of heavy metals result in the contamination of the environment by these metals. Excess concentration of these metal ions in the environment comes from various natural occurrences and human activities such as mining, and industrial discharge. As these metal ions enter into the food chain cause gradual accumulation in living organisms and can cause severe harm to the biological environment¹. Therefore monitoring these ions in the environment is crucial.

Selective detection of metal ions can be effectively carried out by highly selective molecular species known as chemosensors². Metal based functional materials like chemosensors have potential applications in wide areas such as biology, environmental science, analytical chemistry and medical science. Metal sensors play a vital role in the low cost detection of essential and hazardous metals like Hg, Zn, Cd, Fe, Cu and Th.

Metal-organic frameworks (MOFs) are highly sensitive and selective to various energy and charge transfers that take place among ligands as well as metal centres. MOFs based chemical sensors show excellent electrochemical responses and turn on and turn off luminescent responses towards various metal ions, molecules, temperature, pH and humidity³. MOFs are porous coordination polymers (PCPs) of diverse structures and large surface area that are characterised by high porosity and excellent adsorption affinities. MOFs possess unique optical properties that qualify them as optoelectronic sensors. The chemical sensors are used for the detection of transition metal ions such as Fe (III), Cu (II), Zn (II), Cr (VI), Pb (II) and Hg (II). MOF-based sensors are successful in the detection of various anions such as CN⁻,

Chapter-6

PO_4^{2-} , NO_2^- , CO_3^{2-} , $\text{Cr}_2\text{O}_7^{2-}$ and CrO_4^{2-} . MOF-based biosensors have been devised for detecting biological molecules like bacterial endospores and human serum albumin. Even slight pH changes occurring in the biological environment can be easily monitored by fluorescence based pH probes. Luminescent thermometers are based on the temperature dependence of luminescence.

Various fluorescent sensors with high selectivity and sensitivity have been developed for metal ion detection, out of which fluorene based metal sensors are vital due to their well-known photophysical properties².

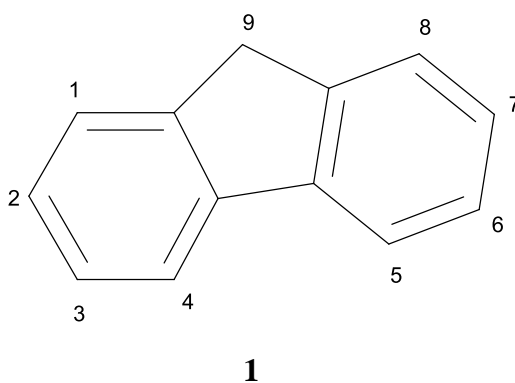


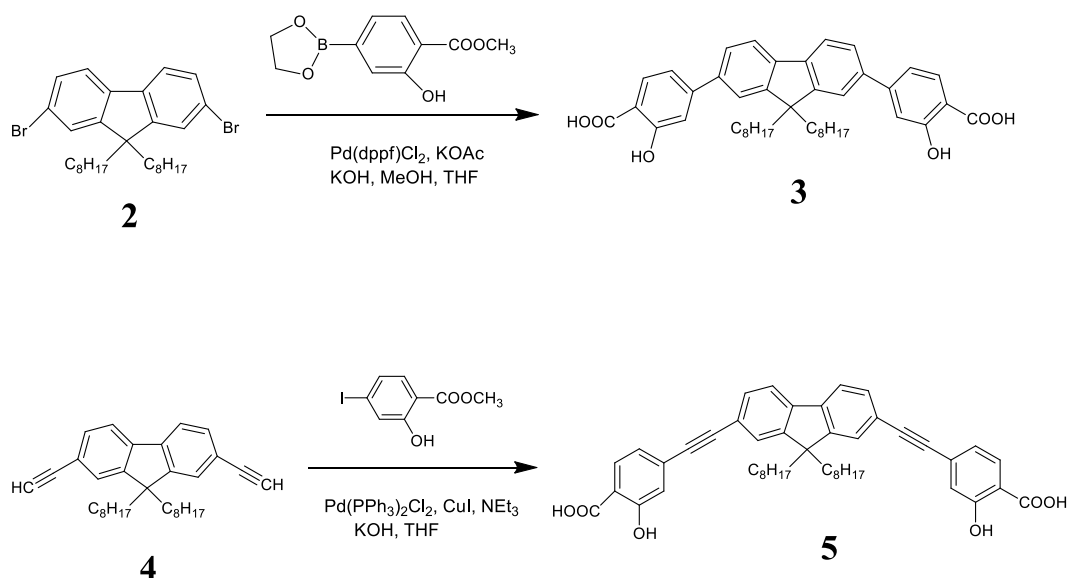
Fig. 1 *Structure of Fluorene*

The fluorene molecule (**Fig. 1**) with molecular formula $\text{C}_{13}\text{H}_{10}$ is an aromatic hydrocarbon consisting of two benzene rings that are joined together through a direct carbon-carbon bond and a methylene bridge⁴. The methylene bridge maintains the planarity of the molecule. Proton at the 9th position of fluorene is highly acidic since the fluorenyl anion formed is aromatic and resonance stabilised. Moreover, the introduction of side groups at position-9 of fluorene increases the solubility of fluorene in common organic solvents.

Molecular design and synthesis concentrate on developing various molecular materials especially conjugated organic chromophores containing metal ions. Metal centres play a great role in governing the properties of fluorene derivatives. Fluorenyl chromophores such as oligofluorenes and polyfluorenes contribute significantly to the field of synthesis of electronic and optoelectronic materials⁵.

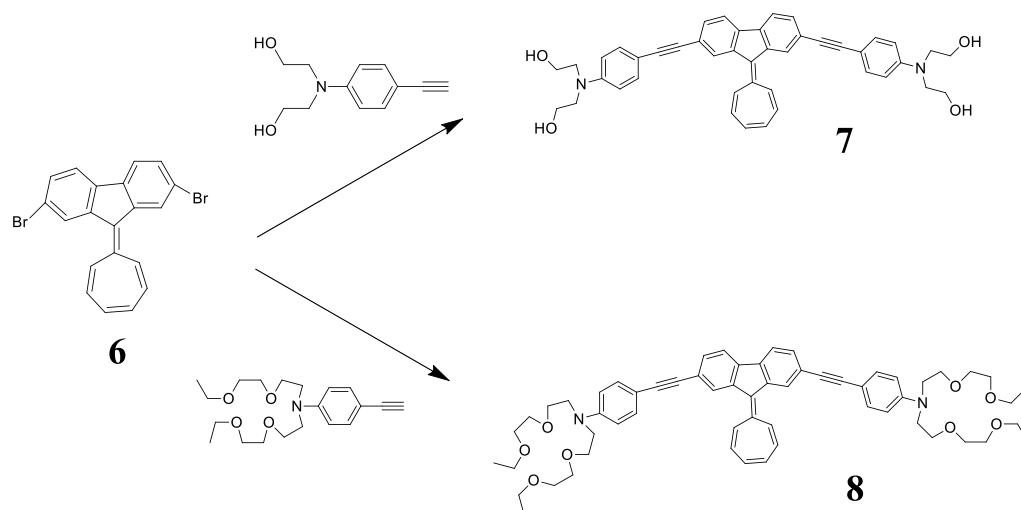
6.2 Synthesis of fluorescent compounds

Water soluble salicylic acid functionalized fluorene derivatives **3** and **5** were synthesised by palladium catalysed Suzuki and Sonogashira coupling reaction⁶ (**Scheme 1**). The salicyl fluorene chemosensor having alkynyl salicylate group **5** exhibits fluorescence quenching selectively towards Fe^{2+} and Cu^{2+} ions.



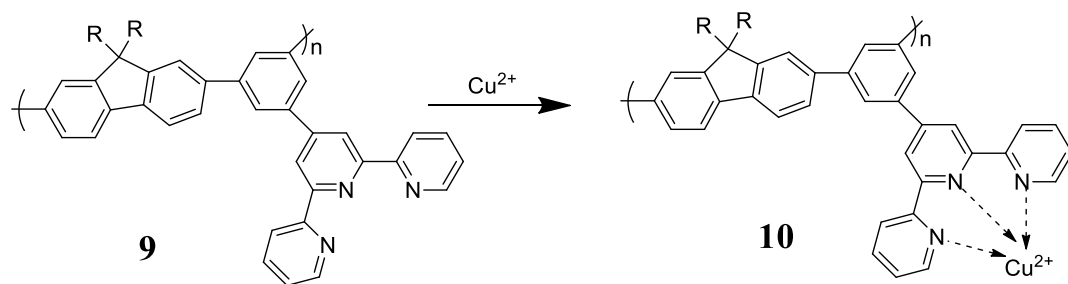
Scheme 1

The detection method based on fluorescent sensors is found to be the most advantageous due to its sensitivity, tunability and ease of detection. Wang *et al.* developed 9-(cycloheptatrienyldene)fluorene derivatives for the effective detection of Fe^{3+} and Cu^{2+} ions⁷. These compounds are of special interest since compound **7** displays enhanced emission with Fe^{3+} in its methanol solution or Cu^{2+} in its acetonitrile solution, whereas compound **8** displays quenched emission with Fe^{3+} or Cu^{2+} in its acetonitrile solution (**Scheme 2**).



Scheme 2

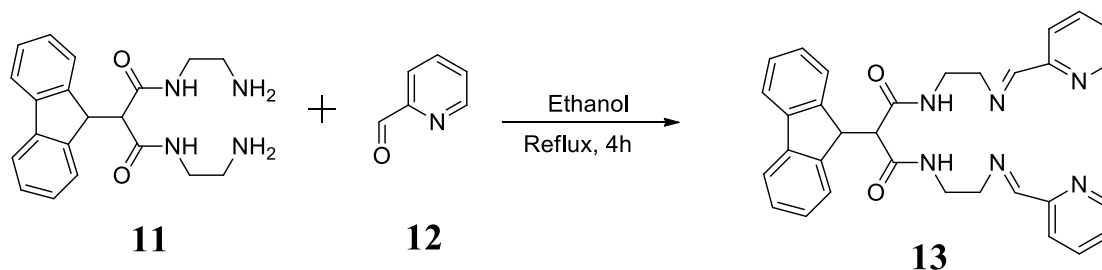
Highly soluble turn-off fluorescent sensor **9** consisting of π -conjugated copolymer with pendant terpyridyl groups, has been synthesised by Suzuki coupling reaction using Pd(0) as catalyst⁸. The fluorescent chemosensor was found to exhibit high sensitivity and selectivity for on-site detection of Cu^{2+} by quenching of fluorescence. Solubility of the sensor in common organic solvents has been increased by the introduction of octyl or 2-(2-(2-methoxyethoxy)ethoxy)ethyl group at the 9th position of fluorene (**Scheme 3**).



Scheme 3

Schiff-base fluorescent sensor **13**, 6-(9-fluorenyl)-1,4,8,11-tetraazaundecane-5,7-dione-1,11-bis(2-iminepyridine), was synthesised from 2-formyl pyridine and 6-(9-fluorenyl)-1,4,8,11-tetraazaundecane-5,7-dione² (**Scheme 4**). The luminescent

sensor exhibited fluorescence quenching selectively for Cu^{2+} ions in dimethyl sulphoxide solution over other metal ions.



Scheme 4

Phosphonic acid functionalized fluorene derivatives **14** and **15** (Fig. 2) are highly efficient chemosensors for the selective detection of Fe^{3+} ions⁹. Fluorescence quenching of **14** and **15** results from the transformation of these fluorenyl chromophores to nonfluorescent complexes when Fe^{3+} ion bind through oxygen atom present in the phosphonic acid group of these fluorene based chemosensors.

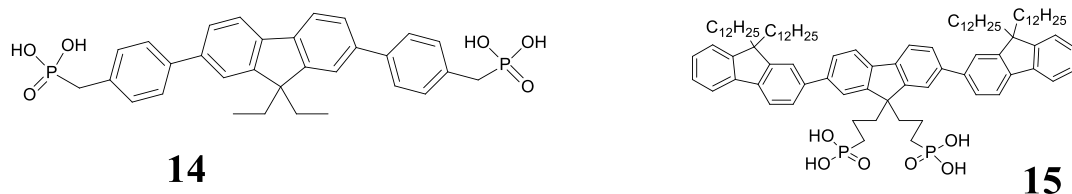
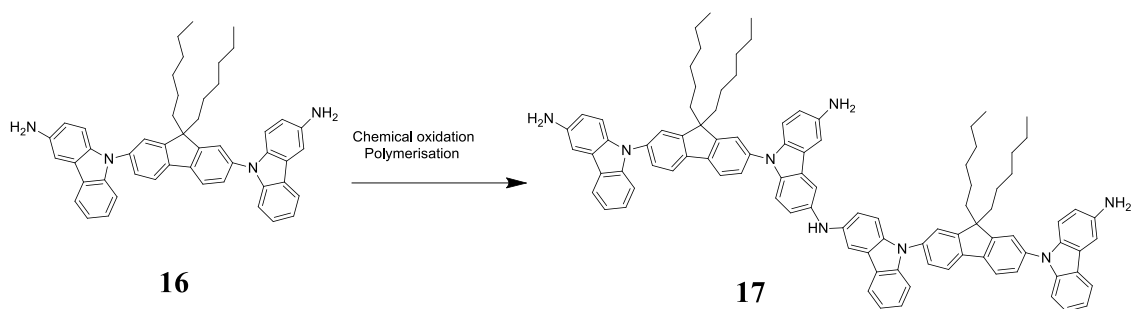
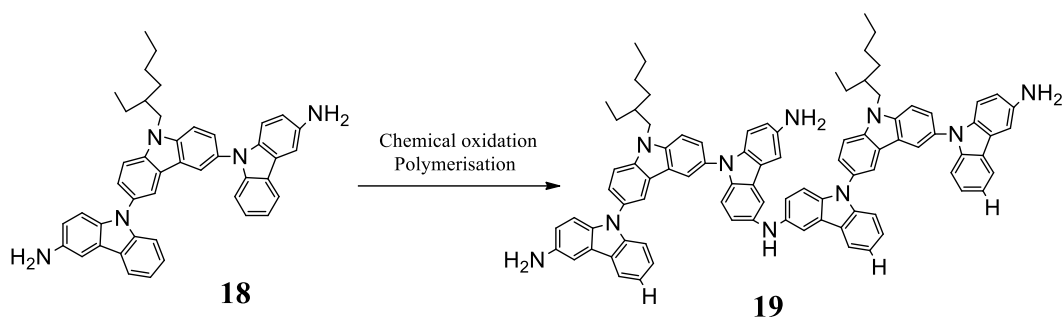


Fig. 2

Polyanilines functionalized with fluorene or carbazole group can be used as fluorescent chemosensors¹⁰. (Poly(9,9^l-(9,9-dihexyl-9H-fluorene-2,7-diyl)bis(9H-carbazol-3-amine))) (PDFCA) **17** composed of fluorene as a central structural unit (**Scheme 5**) and (Poly(S)-9^l-(2-ethylhexyl)-9^lH-[9,3^l:6^l,9^{ll}-tercarbazole]-3,3^{ll}-diamine)) (PETDA) **19** composed of carbazole as the core structural unit (**Scheme 6**) were synthesised. PDFCA is a two dimensional nano-layered material finding potential applications in the sensing field. PDFCA can detect Al^{3+} , Cu^{2+} , Fe^{3+} and H^+ by exhibiting fluorescence quenching. PDFCA is a better chemosensor than PETDA.



Scheme 5



Scheme 6

Since zinc ion play a vital role in biological systems, the detection of Zn^{2+} ions is extremely important. Fluorene derived metal ion sensing probe **20** (Fig. 3) with two photon absorption properties was developed for the detection of Zn^{2+} ions¹¹. The selectivity and sensitivity of the probe were investigated by absorption and fluorescence titration. The sensor possesses a macrocyclic ligand, attached to fluorene backbone that shows preferential binding for Zn^{2+} ions.

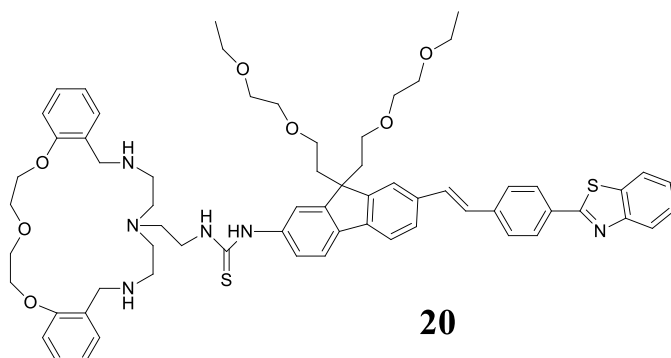


Fig. 3

Cadmium ion is extremely poisonous and various methods have been developed for its detection. Among these, fluorescent sensors are proven to be the best choice due to their low cost, high sensitivity, high selectivity and low detection limits. Moreover, it is easy to apply, safe and found to be free from any interference. Fluorene derivatives are the best choice as sensors due to their rigid planar structure with extended conjugation that imparts interesting electronic properties and large band gap, responsible for highly intense blue fluorescence.

The π -conjugated aromatic rings and various binding sites present in fluorene derivatives impart extraordinary fluorescence properties to these molecules that enable them to be used as chemosensors. The Fluorescence being pH dependent, these chemosensors detect different ions at different pH ranges. Superparamagnetic iron oxide nanoparticles (SPIONs) functionalized fluorescent fluorene chemosensors **21** (Fig. 4) have been developed for the selective sensing of cadmium ions¹. A red-shifted fluorescence at neutral pH indicates the presence of Cd^{2+} ions. The concentration dependence of fluorescence is illustrated by increased fluorescence intensity with the increase in the concentration of Cd^{2+} ions. The fluorescence signal is the indication of intermolecular charge transfer (ICT) that occurs from fluorene derivative to metal ion. Carboxylic sites in the fluorene chemosensors are the binding sites for Cd^{2+} ions in dimethylformamide solution. The presence of cyano group can further enhance the intensity of fluorescence by withdrawing the charge transfer to binding sites. The fluorene chemosensors are coated with SPIONs to improve their solubility in dimethylformamide and also to increase fluorescence intensity.

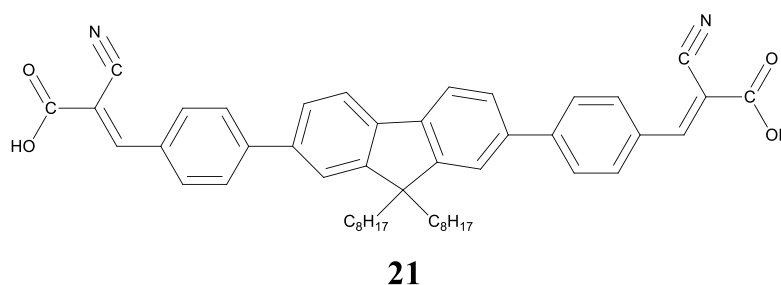
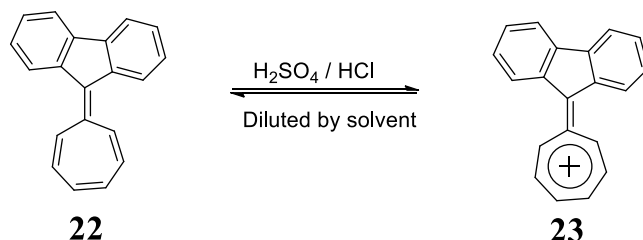


Fig. 4

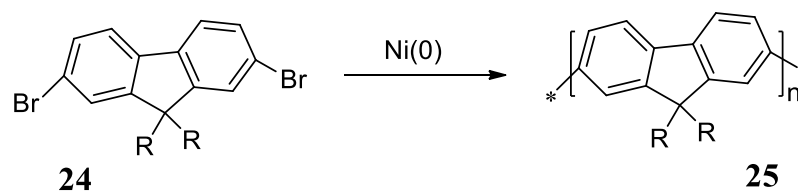
Detection of mercury is very important since the presence of a very low concentration of mercury itself is very dangerous to biological systems. Min *et al.* developed a technique for the detection of Hg^{2+} ions using a rhodamine-fluorene based dual channel probe¹². Non-fluorescent and colourless rhodamine derivatives produce distinct colours and strong fluorescence upon binding with Hg^{2+} ions. In the presence of mercury ion, ring opening of rhodamine takes place which is indicated by yellow fluorescence along with the change of colour from colourless to pink.

Zixing *et al.* reported acid sensing fluorophore. The pH dependent molecular sensor is based on the reversible equilibrium between 9-(cycloheptatrienylydene)fluorene **22** and its protonated form **23** in a mixture of sulphuric acid and ethanol¹³ (**Scheme 7**). The proposed equilibrium being pH dependent, the switchable molecular system may be used as a pH dependent molecular sensor. In the acidic medium, the colour of the solution changes from orange to colourless due to the protonation of the molecule 9-(cycloheptatrienylydene)fluorene. In the basic medium deprotonation of the protonated species occurs which is indicated by the appearance of orange colour of the solution.

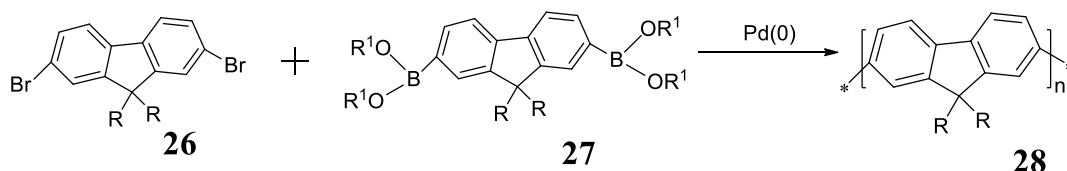


Scheme 7

Aromatic coupling of fluorene monomers at positions 2 and 7 of fluorene yields oligofluorenes. Oligofluorene (OFs) and polyfluorenes (PLs) were synthesised by Ni(0) mediated Yamamoto condensation (**Scheme 8**) or Pd-catalysed Suzuki condensation (**Scheme 9**). Oligofluorenes absorb in the UV region due to π - π^* transition and emit blue light contributing optical properties to the molecule. Polyfluorenes exhibiting optoelectronic properties find applications in polymer electronic devices⁴.



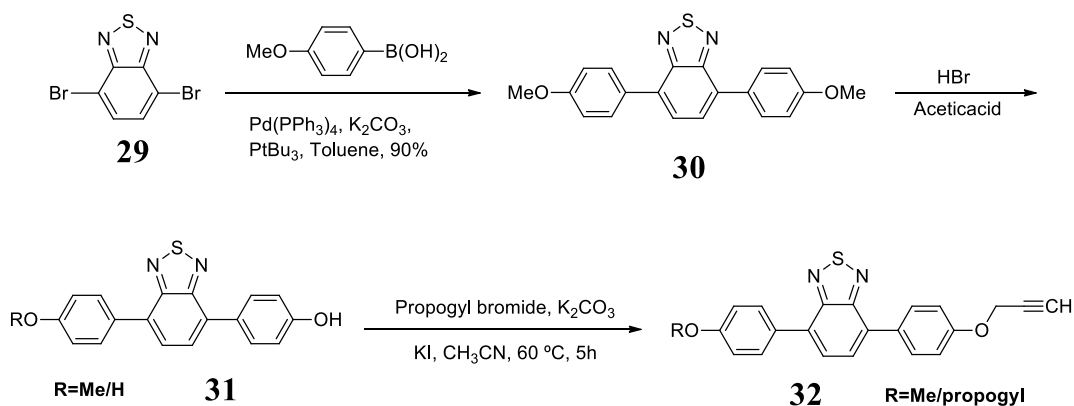
Scheme 8



Scheme 9

Fluorene derivatives with high glass transition temperature and good thermal stability can be suitably fabricated to the organic light emitting diodes (OLEDs) having high current efficiency and power efficiency¹⁴. The fluorescence of fluorene compounds is tunable across the full visible range by changing the extent of conjugation or changing the donor acceptor strength. These features make them good precursors for organic light emitting diodes (OLEDs) and for developing multicolour light emitting materials for colour displays.

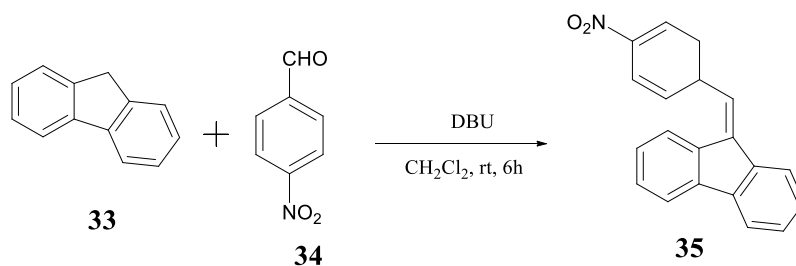
Highly fluorescent 2,1,3-benzothiadiazole derivatives were synthesised by Omer *et al.*¹⁵. It was reported that these compounds produce strong green electrogenerated chemiluminescence (ECL) in non-aqueous solutions which is visible by the naked eye. 4,7-Dibromo-2,1,3-benzothiadiazole **29** and 4-methoxyphenylboronic acid undergo Suzuki coupling reaction in the presence of the catalytic amount of Pd(PPh₃)₄ and PtBu₃ to get compound **30**. This on selective monodeprotection or dideprotection using excess HBr in acetic acid provided compound **31**. Treatment of **31** with propargyl bromide, K₂CO₃ and a catalytic amount of KI (10 mol %) in acetonitrile at 60 °C for 5h afforded **32** (Scheme 10).



Scheme 10

Conjugated polymers (CPs) used as fluorescent sensors are known as amplifying fluorescent polymers (AFPS)¹⁶. The amplification (increased sensitivity) is due to the ability of conjugated polymers to act as an efficient transport medium for electronically excited states. Photo induced electron transfer due to the presence of electron acceptors results in fluorescence quenching.

Rejithamol *et al.* developed a rapid synthesis of benzylidene-fluorene catalysed by DBU¹⁷ (Scheme 11). Condensation reaction between fluorene **33** and aromatic aldehyde **34** afforded the fluorene functionalized derivatives **35** that can be used as chemical sensors and also in organic optoelectronic devices.



Scheme 11

Two-photon absorption (TPA) theory, developed by Geoppert-Mayer, has been effectively applied in synthetic organic chemistry for the synthesis of chemosensors¹⁸. Technologies such as two photon photodynamic cancer therapy, three dimensional optical data storage, two-photon fluorescence imaging and optical switching devices are based on two photon absorption¹⁹. Fluorene derivatives exhibit the two photon absorption (2PA) phenomenon, which is a topic of great

interest in chemistry. Functionalization of fluorene at 2,7 and 9 positions *via* Ulmann amination reaction provide fluorene analogues (**Fig. 5**) that are potential two photon fluorophores¹⁸. The Fluorenyl ring system consists of a π - conjugated system which is thermally and photochemically stable and can be functionalized at 2,7 and 9 positions. The solubility and electronic character of the fluorene analogues can be altered by varying the substituents at these positions. The substituents at positions 2 and 7 account for the electronic character and the substituent at position 9 for the solubility of the fluorene derivatives.

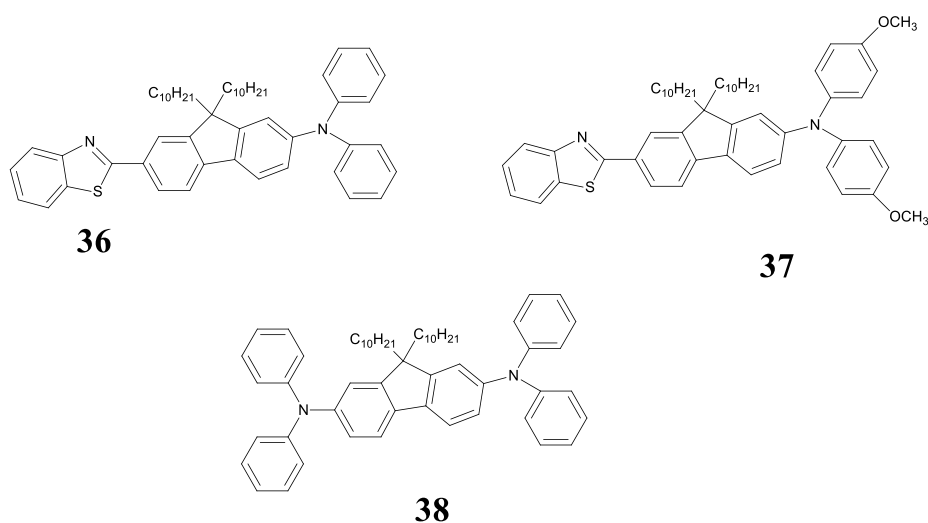
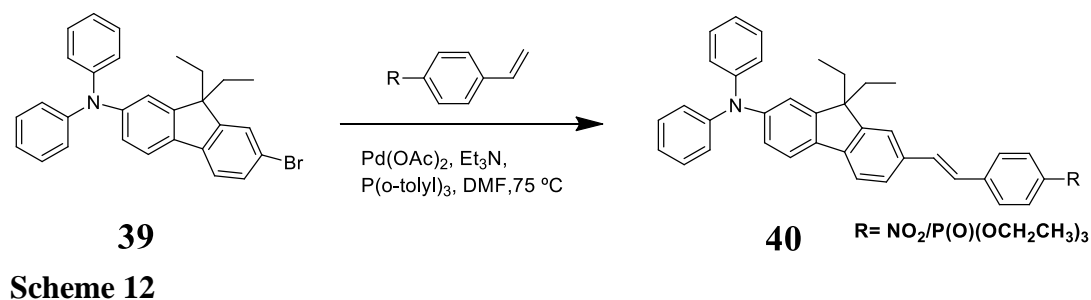


Fig. 5

Belfield reported three dimensional microfabrication employing two photon induced polymerisation. Fluorene dyes **40** were synthesised by Pd-catalysed Heck coupling of 2-bromo-7-N,N-diphenylamino-9,9-diethylfluorene **39** with 4-vinyl benzene phosphonic acid diethyl ester¹⁹ (**Scheme 12**).



Thorium is an actinide element having applications as catalyst, in refractory materials and in the preparation of alloys and nuclear medicines. It finds application in nuclear power generators. Although thorium reactors are extensively used for low cost power generation, thorium contamination of the atmosphere remains a great challenge. Thorium is extremely dangerous to our ecosystem. It is highly carcinogenic and also causes mutation in living organisms. Therefore, monitoring of thorium contamination in the environment is a topic of great interest. Various techniques have been developed for the detection and estimation of thorium, which include gravimetric analysis, chromatographic techniques, titrimetry, electroanalytical techniques and fluorimetry. These techniques are highly expensive, time consuming and require sophisticated instruments. Therefore, the development of a highly sensitive and selective, low cost technique for the detection of thorium is highly desirable. Recently, Kumar *et al.* developed a colourimetric chemosensor for the detection of Th^{4+} ions using tetrabutyl([2,2'-bipyridine]-5,5'-diylbis(methylene))bis(phosphonate) **41** (Fig. 6), a colourless compound which on complexation with Th^{4+} becomes pink coloured²⁰.

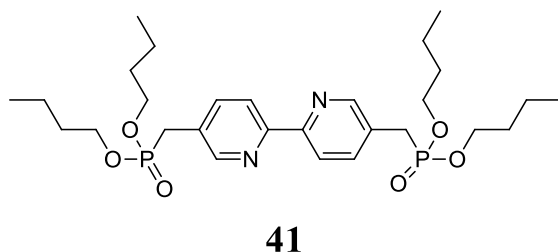
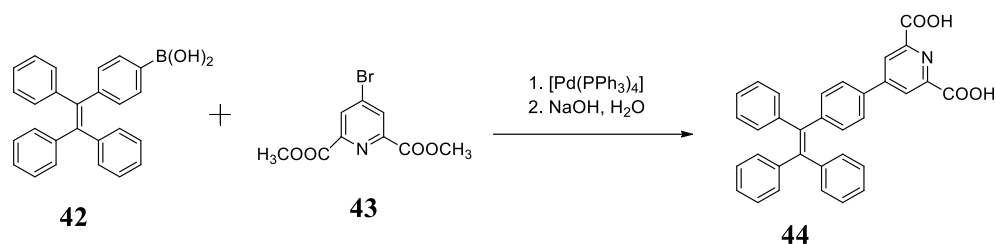


Fig. 6

Aggregation induced emission (AIE) is a useful technique for the highly selective and sensitive recognition of thorium ions. Tetraphenylethene (TPE) substituted with 2,6-pyridine dicarboxylic acid (PDA) is an AIE fluorescent sensor for selective detection of thorium with an enhancement of fluorescence detectable by the naked eye. The chemosensor efficiently recognises thorium among other metal ions under UV light. The AIE active sensor TPE-PDA **44** was synthesised for the detection of thorium in an aqueous solution through Suzuki-Miyaura reaction (Scheme 13)²¹.



Scheme 13

Kuwar *et al.* developed a chemosensor for sensing Th^{4+} ions. The sensor **45** (Fig. 7) on complexation with Th^{4+} ion displayed detectable responses in UV light as well as in fluorescence absorption. The detection limit of the sensor for Th^{4+} ion was reported as $0.1 \mu\text{M}^{22}$.

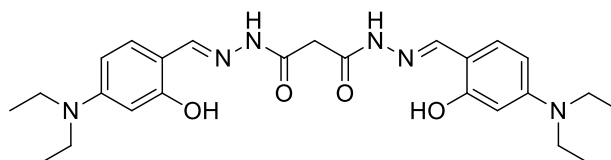


Fig. 7 **45**

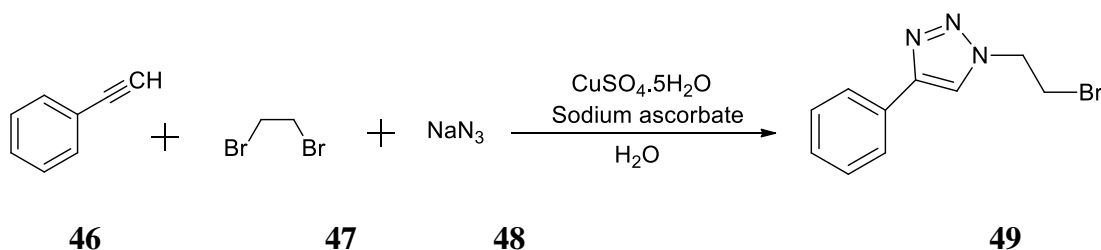
An optical sensing membrane for Th^{4+} ions has been designed by Safavi and Sadeghi. The membrane was developed by incorporating 4-(*p*-nitrophenylazo)-pyrocatechol in the PVC matrix. In the presence of Th^{4+} ion, the yellow coloured membrane became red coloured. This membrane could detect the presence of Th^{4+} ion up to a concentration of $6 \mu\text{M}^{23}$.

Raymond *et al.* synthesised a macrocyclic ligand consisting of terephthalamide units that can effectively chelate with Th^{4+} giving a highly stable complex. The complexation was examined *via* kinetic and spectrophotometric methods. The synthesised ligand being a Th^{4+} ion detector, it has radiotherapeutic applications²⁴.

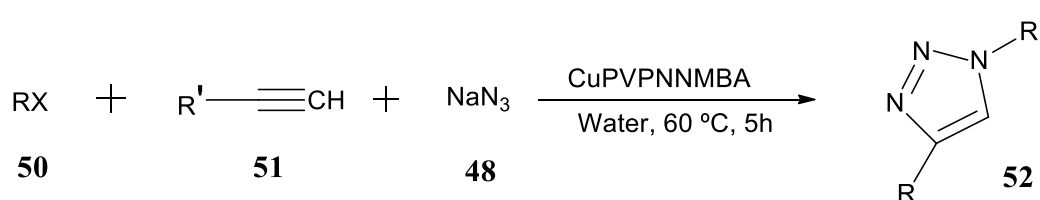
6.3 Results and discussion

1,2,3-Triazoles possess acidic as well as basic characteristics and are easily reducible compounds. These compounds interact with target molecules *via* Van der Waals, hydrogen bonding, dipole-dipole and non-covalent interactions. These compounds can be easily synthesised by 'click' reactions²⁵. Several synthetic routes for triazoles have been reported in the literature. Triazoles **49** were synthesised by simple click reaction between alkyne **46**, dibromoethane **47** and sodium azide **48** in the presence of copper sulphate pentahydrate and sodium ascorbate in the aqueous medium²⁶(Scheme 14).

Alkyl halide **50** and alkyne **51** upon reaction with sodium azide **48**, water and the copper supported polymer catalyst (CuPVPNNMBA) at 60 °C for 5h afford triazole **52** (Scheme 15)²⁷. Radical initiator azobisisobutyronitrile (AIBN) facilitates suspension polymerisation of N-vinyl-2-pyrrolidone (NVP) with N,N'-methylenebis-acrylamide (MBA) to afford CuPVPNNMBA. The catalyst promotes the click reaction between azides and terminal alkynes to afford 1,2,3-triazoles.



Scheme 14



Scheme 15

Triazoles are used as chemosensors for the detection of ions and molecules²⁸. Compounds incorporated with triazole moiety were widely applied for analyte detection in environmental chemistry and biological systems. These triazole functionalized molecules selectively bind with the analyte *via* triazolyl moiety. Such binding results in the enhancement or quenching of fluorescence. Open chain **53** as well as macrocyclic **54** chemosensors having triazole moiety as a binding unit (**Fig. 8**) have been developed²⁹. 1,2,3-Triazoles having hydroxyphenyl group as substituent exhibit fluorescence due to intramolecular charge transfer transitions³⁰.

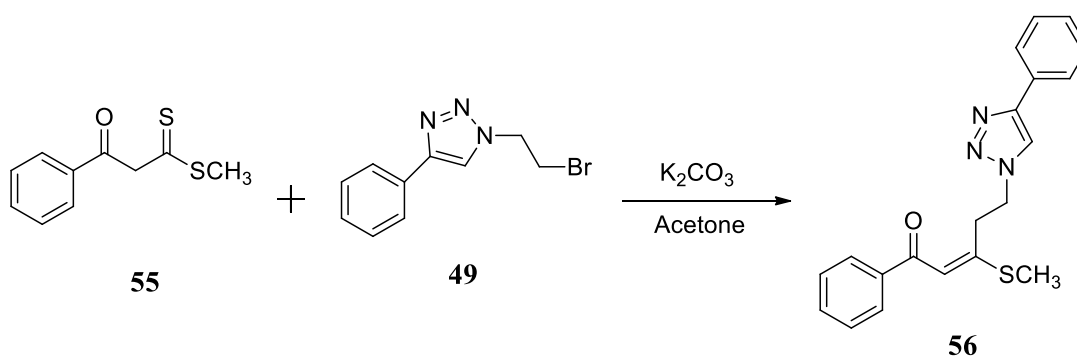


Fig. 8

53

54

Based on the above investigations, we have decided to incorporate triazole moiety into some of the β -oxodithioesters that were synthesised in our laboratory and also to study their fluorescence properties. On this ground, we have synthesised some triazoles and attempted to incorporate them with β -oxodithioester. For this, dithioester **55** was treated with triazole **49** and potassium carbonate in acetone at 50 °C for 2h. (**Scheme 16**). But we failed to get triazole incorporated β -oxodithioesters **56**.



Scheme 16

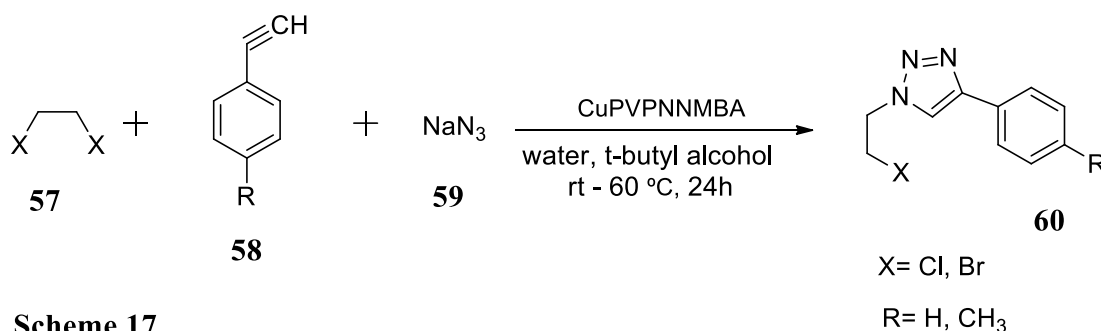
(Expected product)

On this ground, we decided to study the complexation property of triazoles with various d and f-block metal ions. Preliminary studies showed that triazoles exhibit

fluorescence enhancement upon complexation with metal ions. This investigation motivated us to design an efficient fluorescent detector for the selective detection of metal ions. In the present work, simple triazoles, triazole functionalized coumarine, triazole functionalized fluorene and thioamide functionalized fluorene have been synthesised.

6.3.1 Synthesis of triazoles

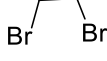
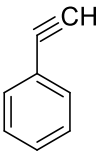
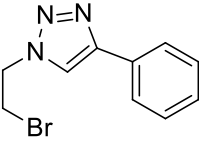
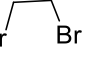
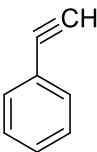
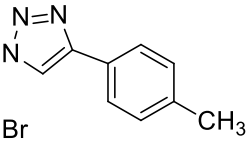
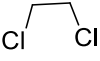
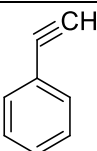
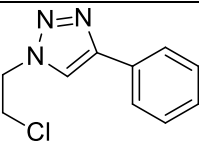
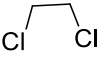
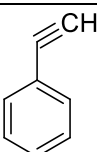
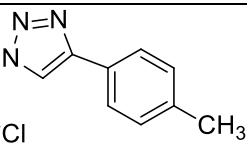
An efficient synthetic protocol for triazoles has been devised. It utilises an excess amount of dihaloethane and copper supported polymer catalyst. In this method, a mixture of dihaloethane **57** (4 eq.), alkyne **58** (1 eq.) and sodium azide **59** (1.5 eq.) was treated with a catalytic amount of copper supported polymer catalyst (CuPVPNNMBA) in a 1:3 mixture of distilled water and t-butyl alcohol. The reactants were stirred at room temperature for 30 minutes and gradually increased the temperature to 60 °C. The reaction proceeded smoothly giving triazoles **60** in good yields within 24h (**Scheme 17**). The results of the synthesis are summarized in **Table 1**. Copper supported polymer catalyst (CuPVPNNMBA) was synthesised according to the procedure which was previously reported by our group²⁷.



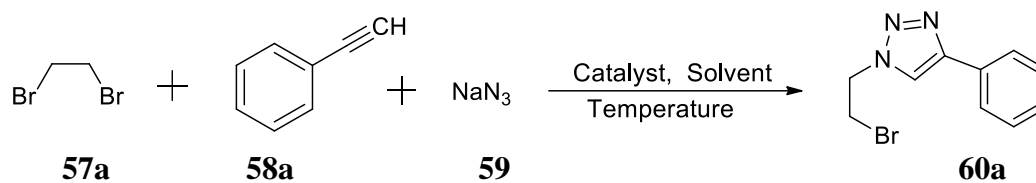
Scheme 17

The reaction between phenylacetylene **58a** (1 eq.) and sodium azide **59** (1.5 eq.) and excess dibromoethane **57a** (4 eq.) in the presence of CuPVPNNMBA as catalyst provided 1-(2-bromoethyl)-4-phenyl-1H-1,2,3-triazole **60a**. The product **60a** showed one proton singlet at δ 7.18 ppm corresponding to hydrogen in the triazole ring. The aromatic hydrogens appeared at δ 7.37-7.18 ppm. The triplets at δ 4.71 and 3.71 ppm were attributed to hydrogens present in the halo ethyl moiety.

Table. 1 1,4-disubstituted 1,2,3-triazoles (**60**):

Sl No.	Alkyl halide (57)	Alkyne (58)	1,2,3-triazoles (60)	Yield (%)
1	 57a	 58a	 60a	90
2	 57a	 58b	 60b	92
3	 57b	 58a	 60c	88
4	 57b	 58b	 60d	90

To optimise the reaction conditions such as temperature, solvent and catalyst loading, the reaction between 1,2-dibromoethane **57a**, phenylacetylene **58a** and sodium azide **59** was carried out in different reaction conditions (**Scheme 18**). The best yield was obtained when the reaction was carried out in the presence of CuPVPNNMBA as the catalyst. The best solvent for the conversion was found to be a 1:3 mixture of H₂O & *t*-butyl alcohol. The yield was maximum when the reaction was started at room temperature and gradually increased the temperature to 60 °C and kept at this temperature for 24h. The optimisation studies are shown in **Table. 2**.



Scheme 18

Table. 2 Effect of temperature, solvent and catalyst for the synthesis of 1,2,3-triazole (**60**):

Sl. No.	Temperature	Solvent	Catalyst	Yield (%)
1	rt	H ₂ O & ^t BuOH (1:3)	(CH ₃ COO) ₂ Cu. H ₂ O & Sodium ascorbate (1:1)	72
2	70 °C	H ₂ O & Acetonitrile (1:2)	CuPVPNNMBA (10mg)	82
3	70 °C	H ₂ O & ^t BuOH (1:3)	CuPVPNNMBA (10mg)	70
4	rt - 80 °C	H ₂ O & ^t BuOH (1:3)	(CH ₃ COO) ₂ Cu. H ₂ O & Sodium ascorbate (1:1)	90
5	rt - 60 °C	H ₂ O & ^t BuOH (1:3)	CuPVPNNMBA (10mg)	92

The structure of the synthesised triazoles was confirmed by FT-IR, ¹H NMR and ¹³C NMR. For the general discussion, 1-(2-bromoethyl)-4-phenyl-1H-1,2,3-triazole (**60a**) (**Fig. 9**) was taken as a representative molecule.

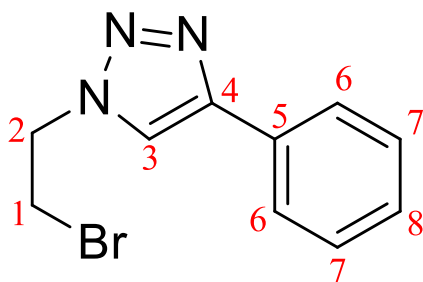


Fig. 9 1-(2-bromoethyl)-4-phenyl-1H-1,2,3-triazole (**60a**)

The FT-IR spectrum (**Fig. 10**) of 1-(2-bromoethyl)-4-phenyl-1H-1,2,3-triazole (**60a**) gives major absorptions at 3049, 2114, 1732, 1452, 1220, 1078, 838, 766, 686, 630 and 518 cm^{-1} . The peaks at 838, 1220 and 1452 cm^{-1} correspond to =C-H, N-N=N and -CH₂ stretching vibrations of the triazole ring. The peaks at 1732 and 3049 cm^{-1} are attributed to aromatic C=C bending and aromatic C-H stretching vibrations respectively. Aromatic C-H bending vibrations were indicated by the signals at 686 and 766 cm^{-1} .

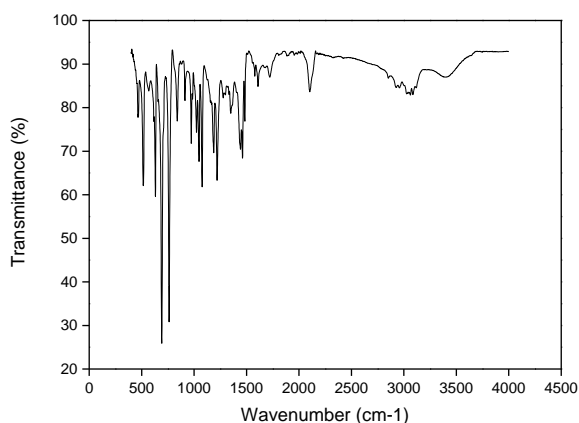


Fig. 10 FT-IR spectrum of 1-(2-bromoethyl)-4-phenyl-1H-1,2,3-triazole (**60a**)

The structure of 1-(2-bromoethyl)-4-phenyl-1H-1,2,3-triazole (**60a**) was confirmed by ¹H NMR spectrum (**Fig. 11**). Two proton triplets at δ 3.71 and 4.71 ppm correspond to protons at positions C1 and C2. The proton at C3 shows one proton singlet at δ 7.84 ppm. The two proton multiplets at δ 7.77-7.75 ppm and δ 7.37-7.27 ppm correspond to protons at C6 and C7 respectively. The proton at C8 was observed as one proton multiplet at δ 7.26-7.24 ppm.

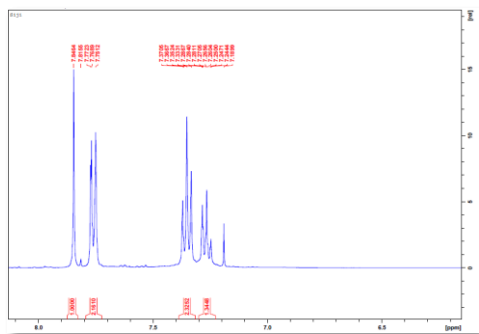


Fig. 11a

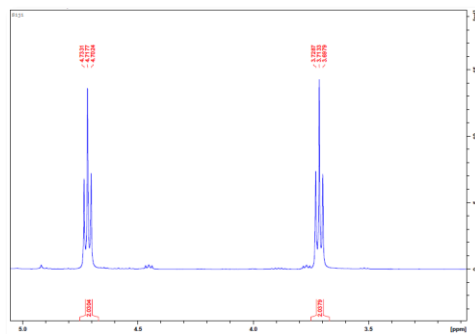


Fig. 11b

Fig. 11 ^1H NMR spectra of 1-(2-bromoethyl)-4-phenyl-1H-1,2,3-triazole (**60a**)

The ^{13}C NMR spectrum of 1-(2-bromoethyl)-4-phenyl-1H-1,2,3-triazole (**60a**) (**Fig. 12**) is in agreement with both FT-IR and ^1H NMR data. The downfield signal at δ 146.4 and 119.5 ppm are due to carbon atoms in the triazole ring. The signals at δ 129.0, 124.6, 127.7 and 127.2 ppm correspond to phenyl carbon atoms C5, C6, C7 and C8 respectively. The signals at δ 28.3 and 50.5 ppm correspond to carbon atoms C1 and C2 respectively in the side chain.

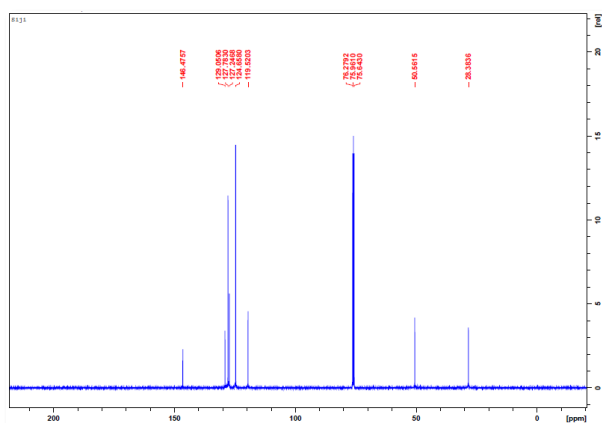


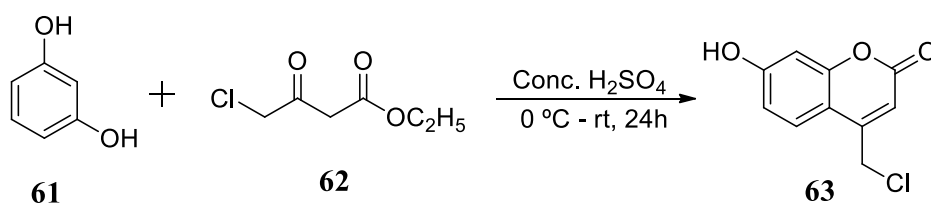
Fig. 12 ^{13}C NMR spectrum of 1-(2-bromoethyl)-4-phenyl-1H-1,2,3-triazole (**60a**)

6.3.2 Synthesis of triazole functionalized coumarin

The fluorescence properties of the synthesised triazoles have been studied and it was found that the fluorescence properties can be enhanced by changing the substituents on the triazole ring. With this insight, we have synthesised

triazole functionalized coumarin **63** and studied its fluorescence properties. The synthesis involves the conversion of resorcinol to coumarin derivative which was then converted to the corresponding triazole.

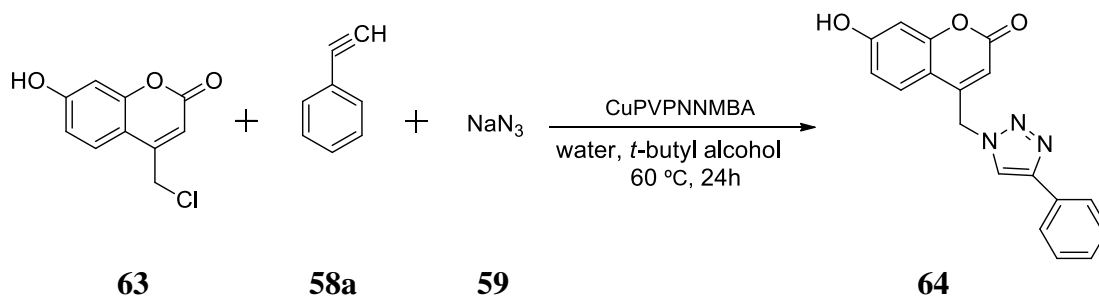
Ethyl-4-chloroacetoacetate **62** (1 eq.) was added to resorcinol **61** (1 eq.) dissolved in conc. H_2SO_4 at $0\text{ }^\circ\text{C}$. The temperature was gradually increased from $0\text{ }^\circ\text{C}$ to room temperature. The mixture was stirred at room temperature for 24h to afford 4(chloromethyl)-7-hydroxy-2H-chromene-2-one **63** (**Scheme 19**).



Scheme 19

Product **63** showed one proton singlet at δ 9.08 ppm corresponding to the hydroxyl group. The aromatic hydrogen peaks appeared in the range δ 6.21-6.71 ppm. The protons of $-\text{CH}_2\text{Cl}$ gave a signal at δ 4.5 ppm. The data is in agreement with that reported in the literature³².

A mixture of 4(chloromethyl)-7-hydroxy-2H-chromene-2-one **63** (1 eq.), phenylacetylene **58a** (1 eq.) and sodium azide **59** (1.5 eq.) was treated with a catalytic amount of copper supported polymer catalyst (CuPVPNNMBA) in a 1:3 mixture of distilled water and *t*-butyl alcohol. The reactants were stirred at room temperature for 30 minutes and gradually increased the temperature to $60\text{ }^\circ\text{C}$. The reaction proceeded smoothly giving triazole functionalized coumarin **64** in good yields within 24h (**Scheme 20**).

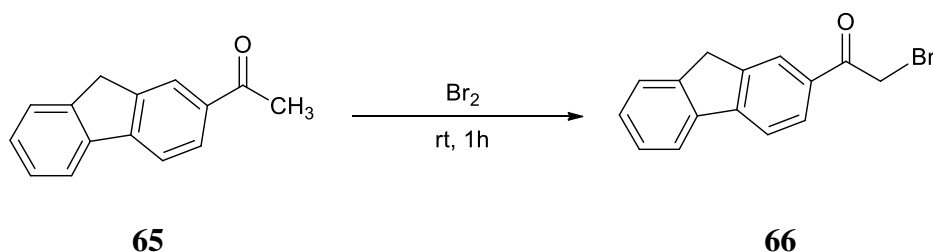


Scheme 20

Product **64** showed one proton singlet at δ 9.08 ppm corresponding to hydrogen in the hydroxyl group. The -CH proton in the triazole ring and the vinylic proton in the coumarin ring are denoted by one proton singlet at δ 8.05 and 6.25 ppm respectively. The -CH₂N protons are denoted by two proton singlet at δ 4.5 ppm. The signals at δ 6.21-6.71 ppm denote aromatic protons in the coumarin ring. The multiplet at δ 7.42-7.47 ppm denotes aromatic protons in the phenyl group attached to the triazole ring. The data is in agreement with that reported in the literature³³.

6.3.3 Synthesis of triazole functionalized fluorene

We have designed a highly fluorescent triazole functionalized fluorene derivative that can be used as a sensor for thorium ions. The synthesis begins with the bromination of 2-acetylfluorene **65** using bromine in acetic acid to afford 2-(bromoacetyl)fluorene **66** (Scheme 21)³³. This was treated with phenylacetylene, sodium azide, copper supported polymer catalyst (CuPVPNNMBA) in distilled water at room temperature for 24h followed by heating at 60°C for 48h to get the triazole functionalized fluorene **67**.



Scheme 21

The structure of 2-(bromoacetyl)fluorene **66** was confirmed by ¹H NMR. Compound **66** exhibited two hydrogen singlets at δ 4.5 ppm indicating the presence of the -CH₂ group. Aromatic protons gave signals in the range δ 7.5-7.8 ppm. The data is in agreement with that reported in the literature³¹.

A mixture of 2-(bromoacetyl)fluorene **66** (1 eq.), phenylacetylene **58a** (1 eq.) and sodium azide **59** (1 eq.) was treated with a catalytic amount of copper supported polymer catalyst (CuPVPNNMBA) in a 1:3 mixture of distilled water and t-butyl alcohol. The reactants were stirred at room temperature for 30 minutes and

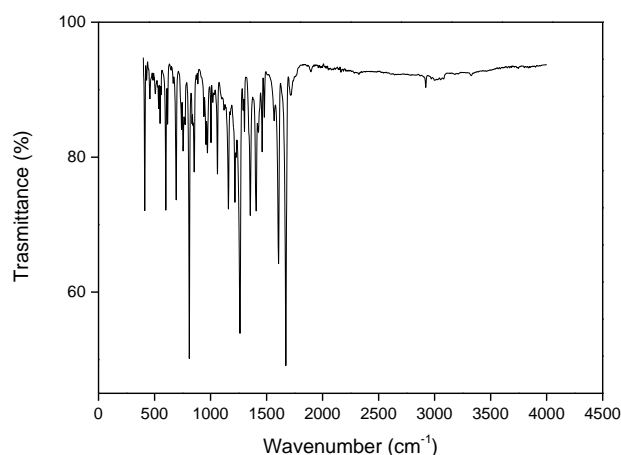


Fig. 14 FT-IR spectrum of triazole functionalized fluorene (**67**)

The structure of the triazole functionalized fluorene **67** was confirmed by the ^1H NMR spectrum (**Fig. 15**). Two proton singlets at δ 2.65 ppm and δ 3.92 ppm correspond to protons at positions C13 and C15 respectively. The signals in the range δ 7.26-8.12 ppm are attributed to aromatic protons.

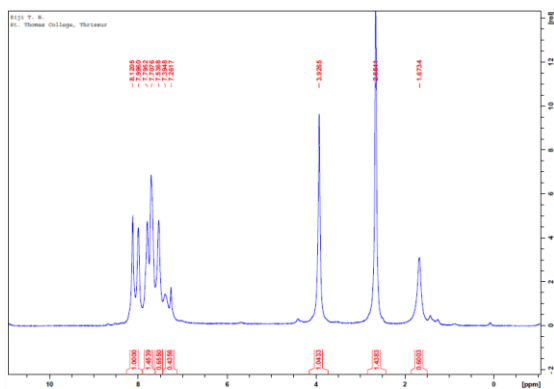


Fig.15 ^1H NMR spectrum of triazole functionalized fluorene (**67**)

The ^{13}C NMR spectrum of the triazole functionalized fluorene **67** (**Fig. 16**) was in agreement with both FT-IR and ^1H NMR data. The downfield at δ 197.8 ppm is due to carbonyl carbon C14. The peaks at δ 146.3 and 120.8 ppm are due to carbon atoms C17 and C16 in the triazole ring. The methylene carbons C13 and C15

give signals at δ 26.7 and 36.7 ppm respectively. The signals at δ 145.3-119.7 ppm are attributed to aromatic carbon atoms.

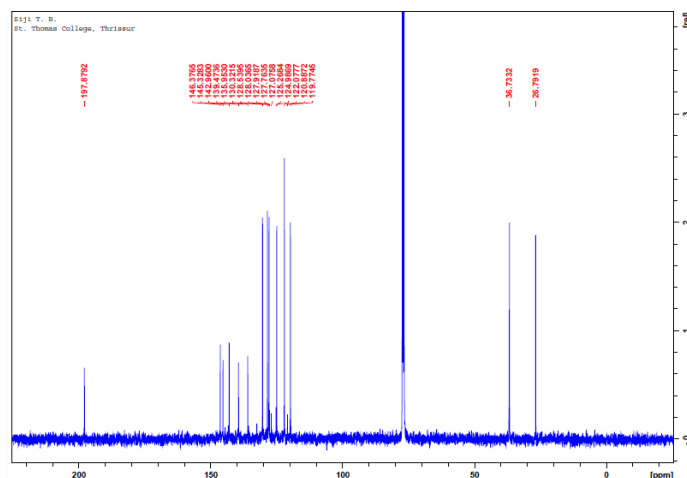


Fig.16 ^{13}C NMR spectrum of triazole functionalized fluorene (**67**)

The structure of the triazole functionalized fluorene **67** was further confirmed by the GCMSMS spectral analysis. The molecular ion peak (M^+) was observed at m/z 351.4 (**Fig. 17**).

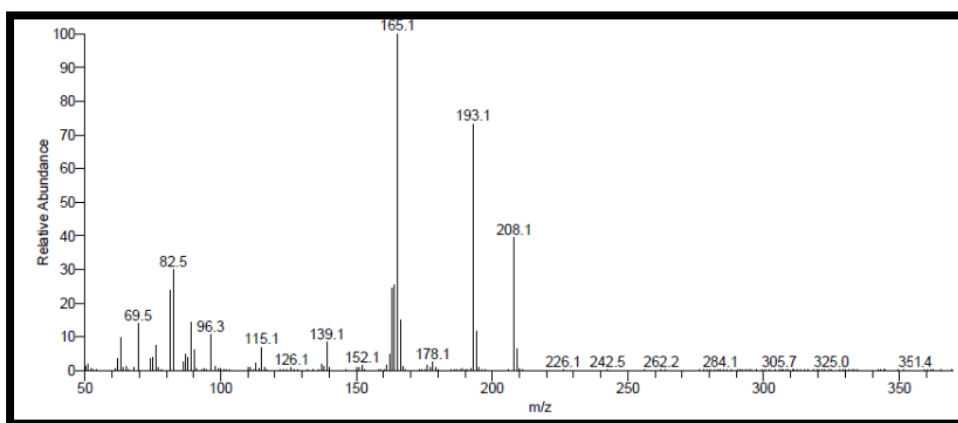
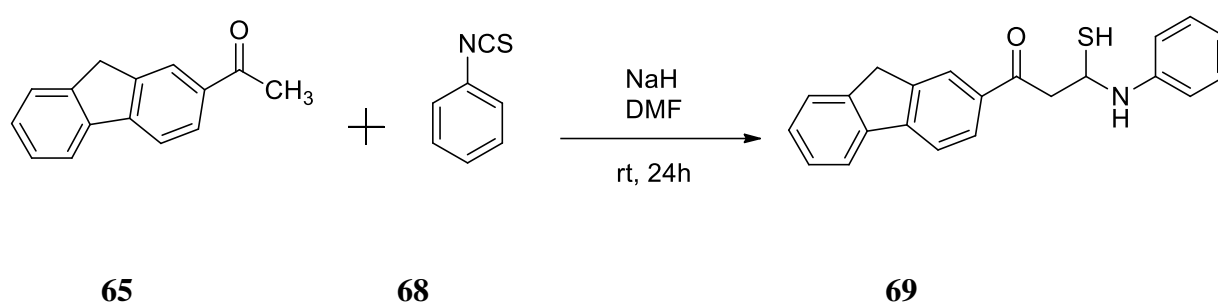


Fig. 17 Mass spectrum of triazole functionalized fluorene (**67**)

6.3.4 Synthesis of thioamide functionalized fluorene

Thioamides exhibit fluorescence properties. Lin *et al.* developed a thioamide based fluorescent probe for Hg^{2+} ions³⁴. In the present work, thioamide functionalized fluorene **69** has been synthesised from 2-acetylfluorene **65**. The reaction between 2-acetylfluorene **65** (1 eq.), phenyl isothiocyanate **68** (1 eq.) and sodium hydride (NaH) (1.7 eq.) in N, N-dimethylformamide (DMF) at room temperature for 20h afforded the thioamide functionalized fluorene **69** (Scheme 23).



Scheme 23

The structure of the thioamide functionalized fluorene **69** (Fig 18) was confirmed by FT-IR, ¹H NMR, ¹³C NMR and GCMSMS analysis.

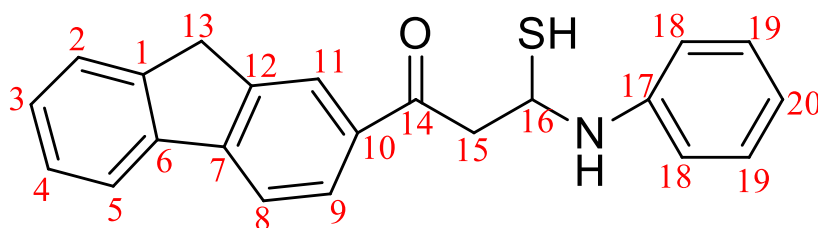


Fig. 18 Thioamide functionalized fluorene (**69**)

The FT-IR spectrum (Fig. 19) of the thioamide functionalized fluorene **69** gives major absorptions at 2934, 2846, 1703, 1671, 1616, 1256, 1192, 1120, 977, 848, 753, 745, 681, and 609 cm^{-1} . The peaks at 1616 and 1192 cm^{-1} correspond respectively to N-H bending and C-N stretching vibrations of secondary amine. The signal due to C=O stretching vibration was observed at 1671 cm^{-1} . The signal at 745 cm^{-1} denotes C-S stretching vibrations. The peaks at 977, 848, 753, 681 and 609 cm^{-1}

are due to aromatic stretching and bending vibrations. The signal at 2934 and 2846 cm^{-1} are attributed to methylene C-H asymmetric and symmetric stretching vibrations respectively.

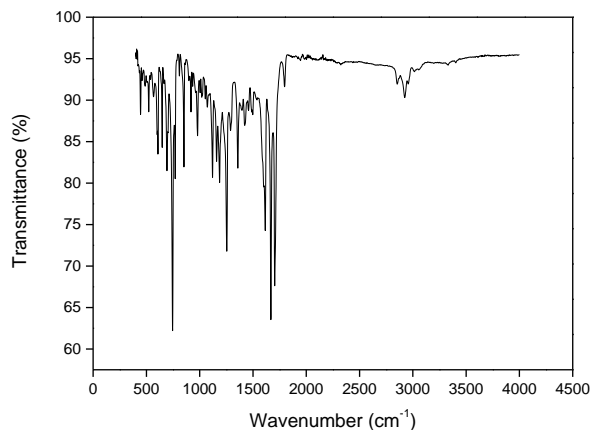


Fig. 19 FT-IR spectrum of thioamide functionalized fluorene (**69**)

The structure of the thioamide functionalized fluorene **69** is confirmed by the ^1H NMR spectrum (**Fig. 20**). Two proton singlets at δ 2.63 and 2.7 ppm correspond to protons at positions C13 and C15 respectively. The proton at C16 is denoted by the signal at δ 5.7 ppm. A one proton singlet at δ 4.1 ppm is attributed to the -NH proton. The -SH proton gives a signal at δ 1.2 ppm. The signals at δ 7.37-8.21 ppm are attributed to aromatic protons.

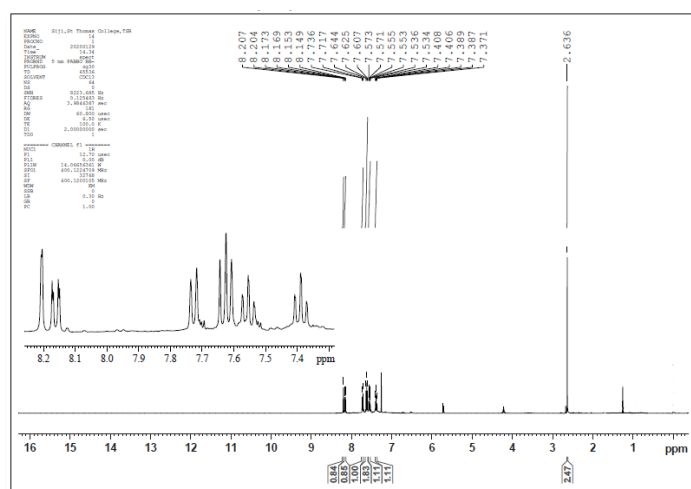


Fig. 20 ^1H NMR spectrum of thioamide functionalized fluorene (**69**)

The ^{13}C NMR spectrum of the thioamide functionalized fluorene **69** (Fig. 21) is in agreement with both FT-IR and ^1H NMR data. The downfield at δ 196.5 ppm is due to carbonyl carbon C14. The carbon atoms C13, C15 and C16 are denoted by the signals at δ 26.6, 30.9 and 60.8 ppm. The signals at δ 148.4-120.4 ppm are attributed to aromatic protons.

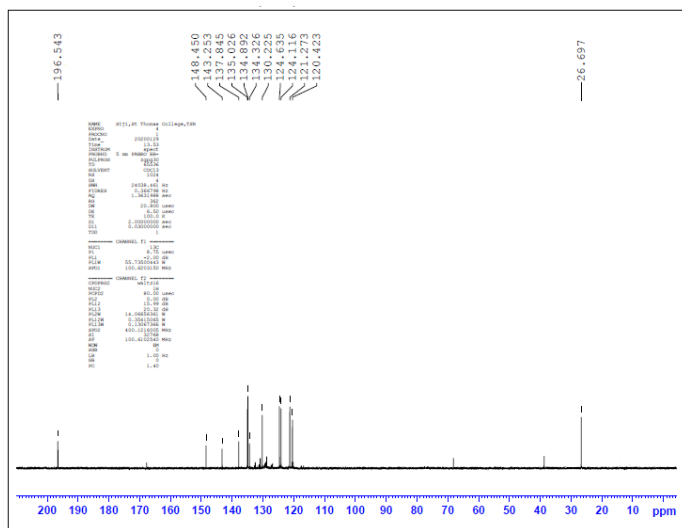


Fig. 21 ^{13}C NMR spectrum of thioamide functionalized fluorene (**69**)

The thioamide functionalized fluorene **69** showed the molecular ion peak (M^+) at m/z 345.5 in GCMSMS spectral analysis (Fig. 22).

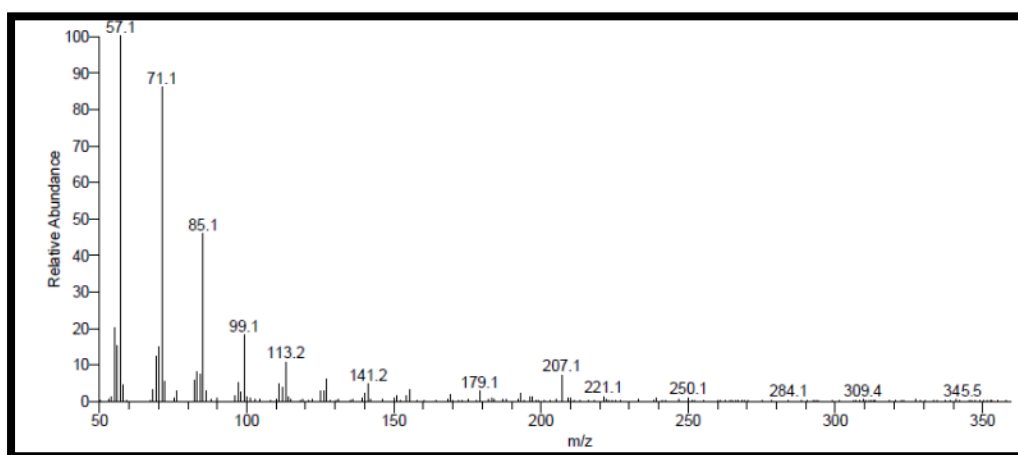


Fig. 22 Mass spectrum of thioamide functionalized fluorene (**69**)

6.4 Fluorescence studies and development of thorium sensor

The triazoles, coumarins as well as fluorene are known to show fluorescence in UV-visible light³⁵. With this perspective in mind, we have synthesised such compounds and studied their fluorescence properties. Variations of fluorescence properties of the compounds upon metal binding have been studied.

The fluorescence enhancement and fluorescence quenching depend on the intramolecular charge transfer (ICT) and energy transfer between the donor and acceptor moieties present in the specific molecule. The charge and energy transfer are extensively influenced by polarity of the solvent, structural environment and conformational relaxation³⁶. Electron withdrawing sulphonyl groups in the fluorene derivatives³⁷ produce charge transfer transitions that result in the decrease of fluorescence quantum yields with increasing solvent polarity. The solvatochromic effect³⁸ was found to be most prominent for symmetrical fluorene derivatives. This is due to the large changes that occurred in the quadrupolar moment of the molecule under excitation. UV-Visible absorption maxima, fluorescence maxima and the on-off property of fluorescence emission are controlled by the solvent polarity³⁹. Even though the intensity of absorption in UV-Visible spectra does not depend much on the solvent polarity, the absorption maxima are found to be red-shifted with solvents of increasing dielectric constants.

In this work, we have studied the fluorescence of triazoles **60**, triazole functionalized coumarin **64**, triazole functionalized fluorene **67**, thioamide functionalized fluorene **69** and their complexes with first row d-block and selected f-block elements. All these compounds, except coumarin functionalized triazole **64**, showed fluorescence enhancement when specifically bind to thorium. In the case of triazole functionalized coumarin **64**, fluorescence quenching was observed (**Fig. 23**). Since the compounds when complexed with thorium exhibited a remarkable fluorescence enhancement, we decided to concentrate on the complexation of the synthesised compounds with thorium (IV) ion in our work.

The studies were carried out in different solvents with varying dielectric constants. The solvents used were acetonitrile, dichloromethane, ethanol and chloroform. It was found that these compounds when dissolved in acetonitrile display fluorescence better than that in any other solvent studied. Therefore, acetonitrile was chosen as the solvent for our study. The solvent effect was most prominent in the case of the triazole functionalized fluorene **67**. The change in fluorescence exhibited by the triazole functionalized fluorene **67** in acetonitrile when complexed with thorium (IV) ion was detectable even by the naked eye.

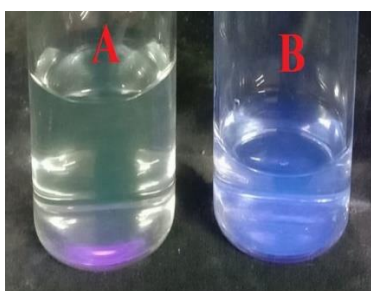


Fig. 23 (a)

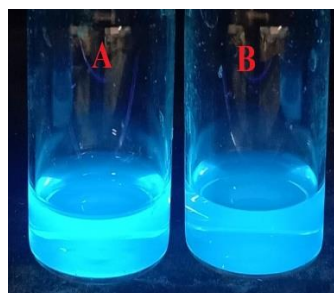


Fig. 23 (b)

Fig. 23 **23a)** Triazole functionalized fluorene **67** (Bottle A) and its complex with Th^{4+} ion (Bottle B); **23b)** Triazole functionalized coumarin **64** (Bottle A) and its complex with Th^{4+} ion (Bottle B)

The UV-Visible absorption properties of the synthesised compounds and their complex with thorium (IV) ion were studied. Fluorescence emission was analysed in UV light at wavelength 365nm using a Rotek UV inspection cabinet (230V). Shimadzu UV-Visible spectrometer (200-800 nm) was used for recording UV-Visible spectra.

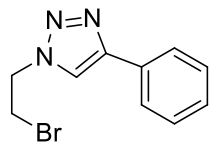
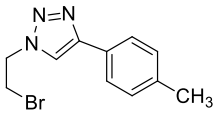
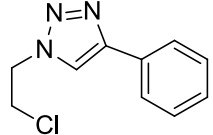
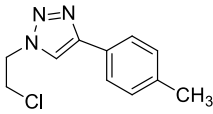
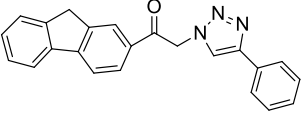
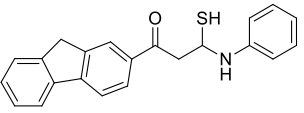
The fluorescence titration method was adopted to study the variation in fluorescence upon complexation and concentration dependence of fluorescence⁴⁰. For this, a stock solution of each of the compounds having concentration 2×10^{-3} M was prepared in acetonitrile and the fluorescence was observed in the UV light. The concentration of the solution giving minimum fluorescence in UV light was determined by diluting the solution using acetonitrile. For this, 1 mL, 2 mL, 3 mL

etc. acetonitrile was added to 5 mL of the stock solution and each time fluorescence emission was analysed. The concentration of the compounds in acetonitrile giving minimum fluorescence was obtained as 6×10^{-5} M for triazole functionalized coumarin **64**, 3×10^{-4} M for triazoles **60b** and **60d**, triazole functionalized fluorene **67** and thioamide functionalized fluorene **69**. The triazoles **60a** and **60c** showed minimum fluorescence at a concentration of 1×10^{-3} M.

The change in fluorescence of the compounds upon complexation with thorium (IV) ion was analysed. For this, a stock solution of thorium (IV) having concentration 2×10^{-3} M was prepared in acetonitrile. Solution of the triazole or fluorene derivative (**60a/60b/60c/60d/64/67/69**) 1 mL each was mixed with 1 mL of the thorium (IV) solution to form the complex and an appropriate volume of acetonitrile was added to the solution so that the resultant concentration of the compound in solution equals that of the minimum fluorescence concentration. The fluorescence of the complex at this concentration was observed in the UV light.

The experiment was repeated by changing the concentration of the thorium (IV) in the solution. The concentration of the thorium required to give minimum fluorescence in UV light keeping the compound concentration at its minimum level was determined. The triazoles **60b** and **60d** could detect thorium even at a low concentration of 1.3×10^{-4} M thorium while the triazoles **60a** and **60c** required 1×10^{-3} M thorium to exhibit fluorescence. Compound **67** exhibited fluorescence even at a low concentration of 3.2×10^{-6} M thorium. Compound **69** showed fluorescence up to 4.3×10^{-5} M thorium. The results of the fluorescence study are summarised in **Table 3**.

Table. 3 Fluorescence emission studies in UV light:

Sl No.	Compound	Minimum molar concentration for fluorescence detection	
		Compound	Thorium ion
1	 60a	1×10^{-3}	1.0×10^{-3}
2	 60b	3×10^{-4}	1.3×10^{-4}
3	 60c	1×10^{-3}	1.0×10^{-3}
4	 60d	3×10^{-4}	1.3×10^{-4}
5	 67	3×10^{-4}	3.2×10^{-6}
6	 69	3×10^{-4}	4.3×10^{-5}

Development of molecular fluorophore for sensing thorium ion

The fluorescence exhibited in the UV light by compound **69** at 3×10^{-4} M concentrations and in the complexed form are depicted in **Fig. 24**. Similarly, the fluorescence of compound **67** at 3×10^{-4} M concentrations and in the complexed form are depicted in **Fig. 25**. The concentration dependence of fluorescence was analysed by observing the fluorescence of the complex (**67** + Th) at different concentrations of thorium (IV) ion. It was found that the intensity of fluorescence increases with an increase in the concentration of thorium. The fluorescence of the complex (**67** + Th) at 1.2×10^{-4} M, 2×10^{-5} M and 3.2×10^{-6} M concentrations of thorium (IV) ion are given in **Fig. 26**.

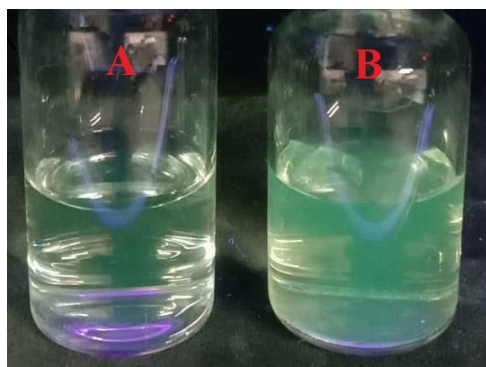


Fig. 24 (1) **Bottle A**- The thioamide functionalized fluorene **69**; (2) **Bottle B**- The thioamide functionalized fluorene **69** complexed with Th^{4+}

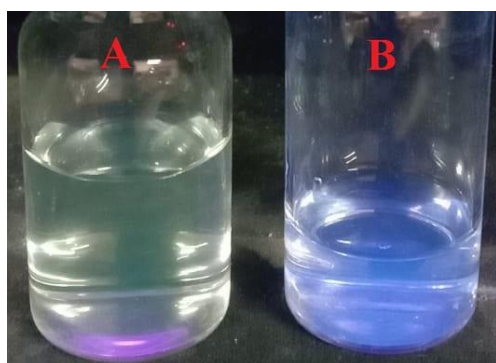


Fig. 25 (1) **Bottle A** - The triazole functionalized fluorene **67**; (2) **Bottle B**- The triazole functionalized fluorene **67** complexed with Th^{4+} ion.



Fig. 26 The Th^{4+} complex of triazole functionalized fluorene **67** at 1.2×10^{-4} M (**Bottle A**), 2×10^{-5} M (**Bottle B**) and 3.2×10^{-6} M (**Bottle C**) concentrations of Th^{4+} ion.

The triazole functionalized fluorene **67** at a concentration of 3×10^{-4} M could detect the presence of thorium at a concentration as low as 3.2×10^{-6} M. Increase in the intensity of fluorescence was observed with an increase in the concentration of thorium (IV) ion. Therefore the triazole functionalized fluorene **67** can be considered an efficient fluorescence detector for thorium (IV) ions at micromolar level.

6.4.1 UV-Visible spectral studies

The UV-Visible absorption spectra of the triazoles (**60a**, **60b**, **60c** and **60d**), triazole functionalized coumarin **64**, fluorene (**67** and **69**) and their complexes with thorium (IV) ion was recorded using UV-Visible spectrometer. The UV-Visible absorption spectra of all the triazoles and their complexes are shown in **Fig. 27**. The UV-Visible absorption spectra of triazole functionalized coumarin **64**, fluorene derivatives (**67** and **69**) and their complexes are depicted in **Fig. 28**. The concentration dependence of fluorescence was studied for the triazole functionalized fluorene **67**. It was found that the intensity of absorption is concentration dependent since it increases with an increase in the concentration of the thorium (IV) ion. The concentration dependence of fluorescence of the Th^{4+} complex of triazole functionalized fluorene **67** is shown in **Fig. 29**.

The wavelength of maximum absorption was determined from the UV-Visible spectra (**Table. 4**). The studies revealed that the wavelength of maximum absorption of the compounds increases upon complexation with thorium (IV) ion.

The compound **60a** exhibited maximum UV absorption at a wavelength of 245 nm. When it was complexed with thorium (IV) ion, the wavelength of maximum absorption slightly shifted to 249 nm. In the case of compound **60b**, the wavelength of maximum absorption shifted from 248 nm to 257 nm upon complexation. The wavelength of maximum absorption for compound **60c** was 244 nm whereas that for its complex was 250 nm. The compound **60d** and its complex absorb at 246 nm and 254 nm respectively. The triazole functionalized coumarin **64** showed maximum absorption at 244 nm and in the complexed form at 251 nm. The triazole functionalized fluorene **67** showed maximum absorption at 314 nm and in the complexed form at 318 nm. The thioamide functionalized fluorene **69** in the uncomplexed and complexed forms were 294 nm and 298 nm respectively.

Table. 4 λ_{max} for compound and complex with thorium (IV) ion:

Entry	Compound	λ_{max} in nm for	
		Compound	Complex
1	60a	245	249
2	60b	248	257
3	60c	244	250
4	60d	246	254
5	64	244	251
6	67	314	318
7	69	294	298

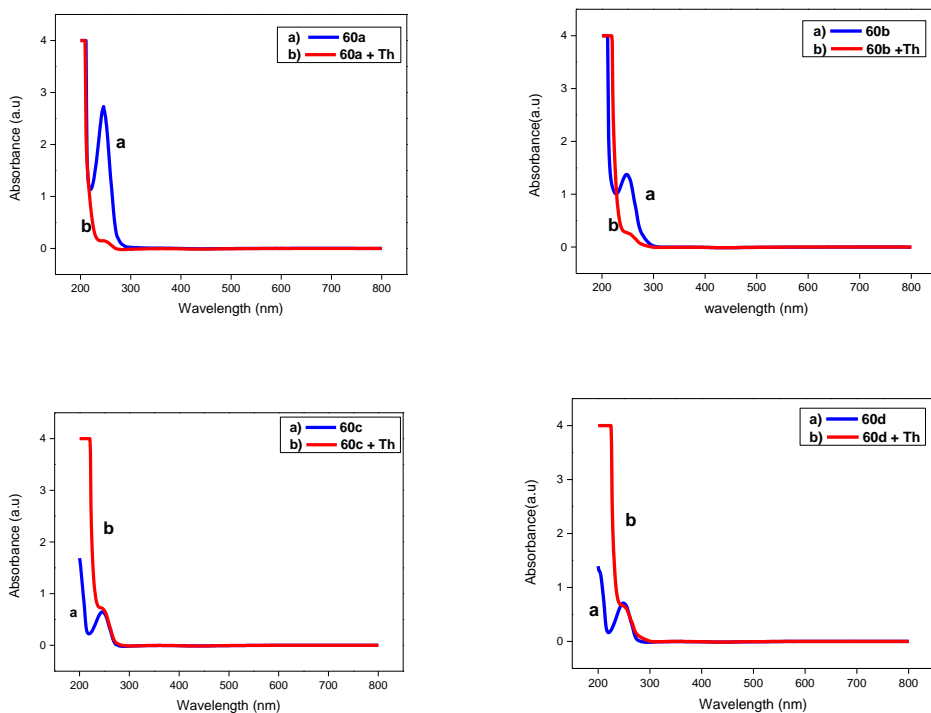


Fig. 27 The UV-Visible absorption spectrum of the triazoles **60** and their Th^{4+} complexes

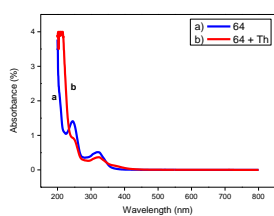


Fig. 28a

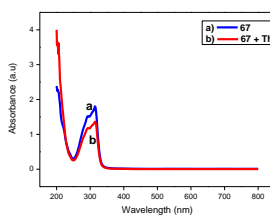


Fig. 28b

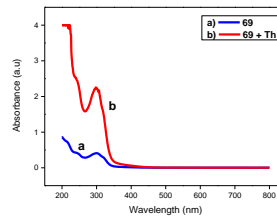


Fig. 28c

Fig. 28 The UV-Visible absorption spectrum of (**28a**) triazole functionalized coumarin **64** and its Th^{4+} complex; (**28b**) triazole functionalized fluorene **67** and its Th^{4+} complex; (**28c**) thioamide functionalized fluorene **69** and its Th^{4+} complex

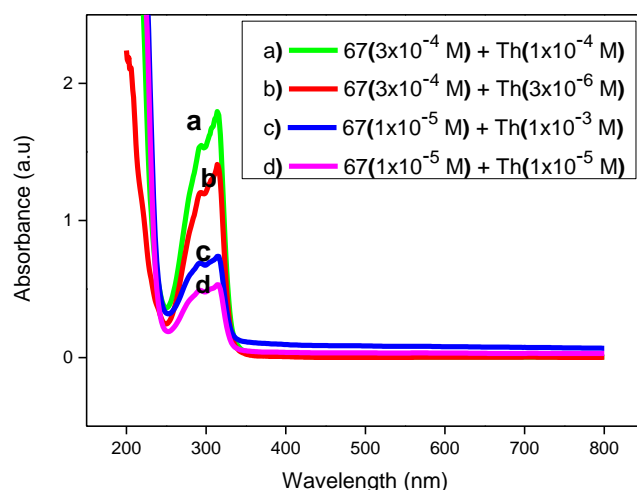


Fig. 29 The UV-Visible absorption spectrum of the Th⁴⁺ complex of triazole functionalized fluorene **67** at different concentrations of compound **67** and Th⁴⁺ ion.

6.4.2 Spectrofluorometric studies

The fluorescence emission studies showed that the triazole functionalized fluorene **67** exhibits remarkable fluorescence shifts on complexation with thorium (IV) ion. Therefore variations in the fluorescence of the triazole functionalized fluorene **67** upon complexation with thorium (IV) ion were further investigated via spectrofluorometric analysis. The fluorescence spectra were recorded by Jasco spectrofluorometer (200-900 nm).

The fluorescence spectra of the triazole functionalized fluorene **67** at a concentration of 3×10^{-4} M and that of the complex (**67** + Th) (**67** = 3×10^{-4} M, Th = 3.2×10^{-6} M) were recorded and found that the intensity of fluorescence increases upon complexation (**Fig. 30**). The fluorescence spectra were recorded at different concentrations of thorium (IV) ion, keeping the concentration of triazole functionalized fluorene **67** at 3×10^{-4} M (**Fig. 31**). The graph showed that the intensity of fluorescence was increased with increase in the concentration of thorium (IV) ion. A red shift in the maximum absorption was observed with an increase in the concentration of thorium (IV) ions in the complex.

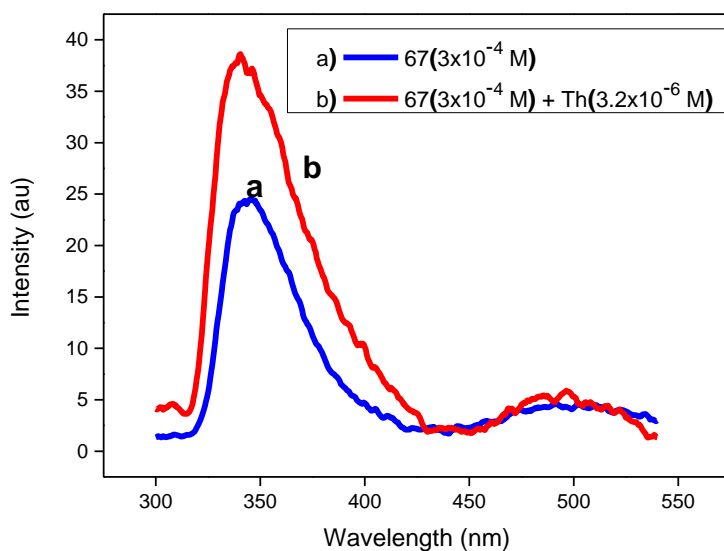


Fig. 30 Fluorescence spectrum of the triazole functionalized fluorene **67** and its Th^{4+} complex.

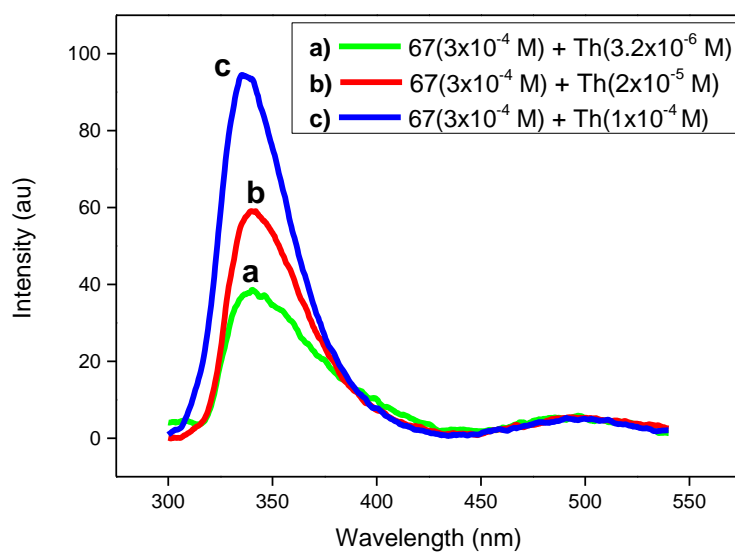


Fig. 31 Fluorescence spectrum of the Th^{4+} complex of triazole functionalized fluorene **67** at different concentrations of Th^{4+} ion

The fluorescence of the complex (**67**+Th) was further analysed by decreasing the concentration of the triazole functionalized fluorene **67** to 1×10^{-4} M in the complex. The triazole functionalized fluorene **67** was mixed with thorium (IV) ion to

form the complexes in which the resultant concentration of the thorium (IV) ion would be 1.4×10^{-4} M and 0.7×10^{-4} M respectively. The fluorescence spectra (**Fig. 32**) recorded in each case showed that the intensity of fluorescence was increased and the wavelength of maximum absorption red shifted with an increase in the concentration of thorium (IV) ion.

A comparison of the spectra of the thorium complex recorded at different concentrations of the triazole functionalized fluorene **67** and Th^{4+} ion showed that the intensity of absorption decreased with the decrease in the concentration of the triazole functionalized fluorene **67** and increased with an increase in the concentration of Th^{4+} ion. As the concentration of the triazole functionalized fluorene **67** decreased, a red shift in the maximum absorption was also observed (**Fig. 33**).

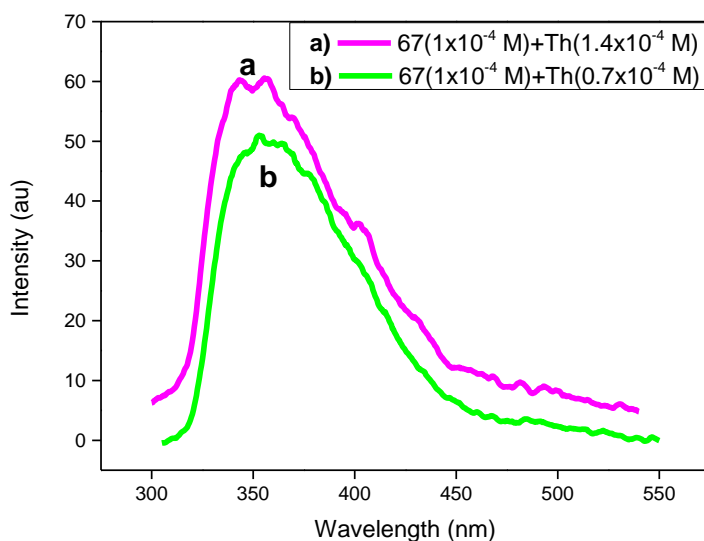


Fig. 32 Fluorescence spectrum of the Th^{4+} complex of triazole functionalized fluorene **67** at different concentrations of Th^{4+} ion

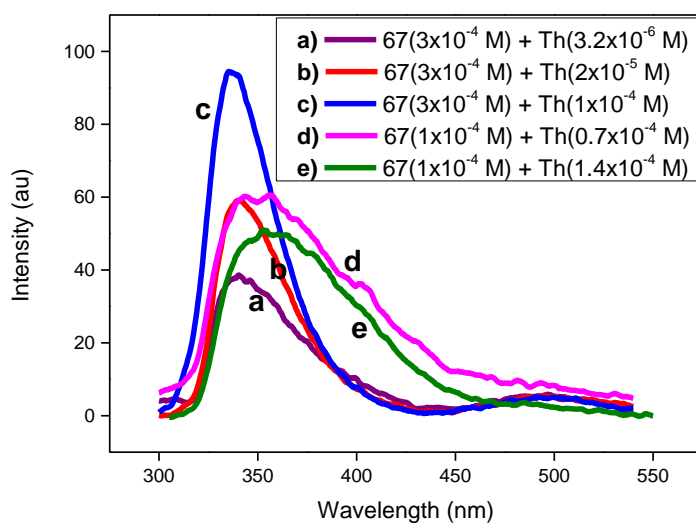


Fig. 33 Fluorescence spectrum of the Th⁴⁺ complex of triazole functionalized fluorene **67** at different concentrations of compound **67** and Th⁴⁺ ion.

6.4.3 Theoretical Calculations

The quantum mechanical calculations were carried out with the Gaussian 09 software package⁴¹. The ground state geometry optimisation of the triazole functionalized fluorene **67** was performed using the BP86/Def2-SVP level of theory⁴². The single-point calculations on the resulting equilibrium geometry have been carried out using the M06/Def2-TZVPP level of theory⁴³. The optimised geometry of the triazole functionalized fluorene **67** shows that the planar fluorene ring makes a dihedral angle of 55.6° with the plane of the triazole-phenyl unit, providing an overall bent molecular geometry (**Fig. 34**).

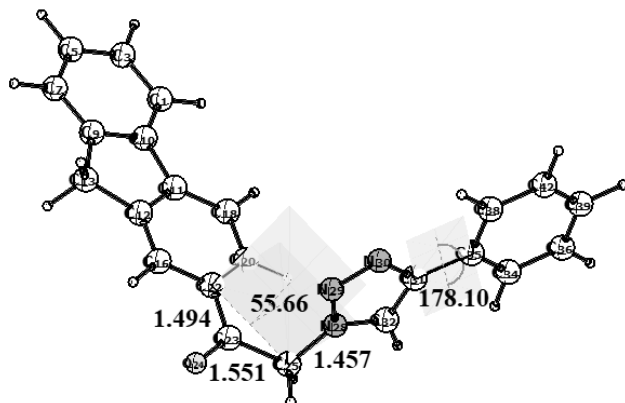


Fig. 34 Optimised geometry of triazole functionalized fluorene **67** at BP86/Def2-SVP level of theory. All angles are given in degrees and bond lengths in Å.

The molecular orbital analysis shows that the highest occupied molecular orbital (HOMO) and lowest unoccupied molecular orbital (LUMO) represent the π and π^* orbital on the fluorene ring and the HOMO-1 and LUMO+1 orbitals correspond to the π and π^* orbital on the triazole-phenyl unit. The HOMO-5 orbital represents the lone pair on the carbonyl oxygen (**Fig. 35**).

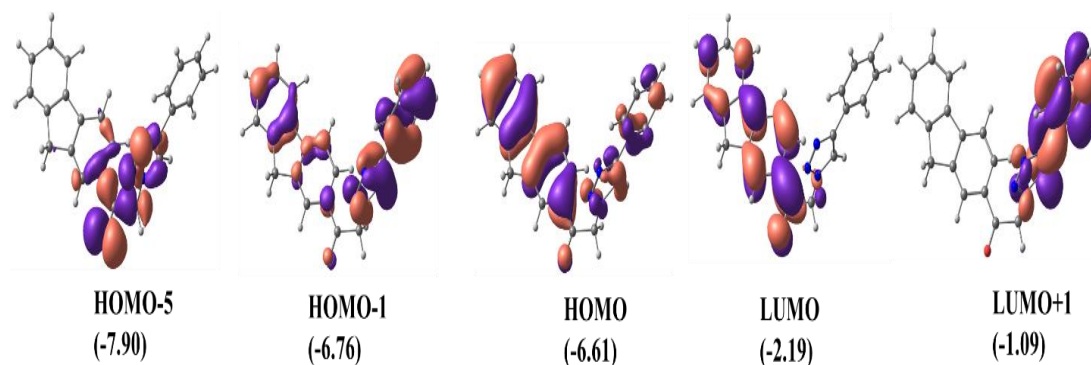


Fig. 35 Selected molecular orbitals of the triazole functionalized fluorene **67** at the M06/def2-TZVPP//BP86/def2-SVP level of theory in acetonitrile. Eigenvalues are given in eV in parentheses. The surfaces are plotted at the iso-surface value of 0.03.

To account for the UV-Visible spectral responses, we have performed the TDDFT⁴⁴ calculations at the M06/Def2-TZVPP level of the Gaussian 09 program using the PCM solvent model⁴⁵ in acetonitrile solvent. The UV-Visible absorption spectrum of the compound exhibits a peak at 300 nm in acetonitrile, which can be assigned to the $\pi \rightarrow \pi^*$ transition (HOMO \rightarrow LUMO transition) in the fluorene ring ($\lambda_{max} = 338$ nm, $f = 0.61$). Moreover, the marginally Stoke-shifted emission band at 350 nm can be attributed to the LUMO \rightarrow HOMO transition (**Fig. 36a, Table 5**). The calculated absorption spectrum of the compound in the gas phase provides the transition at $\lambda_{max} = 325$ nm ($f = 0.31$) which corresponds to the fluorene-triazole $\pi \rightarrow$ fluorene π^* transition (HOMO \rightarrow LUMO transition) (**Fig 36b, Table 5**).

Table 5. The electronic transitions of triazole functionalized fluorene **67** in the ground state in the gas phase and acetonitrile (PCM solvent model) - calculated at M06/def2-TZVPP//BP86/def2-SVP level of theory.

Compound	Oscillator strength (f)	Excitation energy (eV)	Wavelength (nm)	Transition	Coefficient of transition	Percentage contribution
Triazole functionalized fluorene 67 (gas phase)	0.0997	3.69	335.78	HOMO-6→LUMO	0.2042	8.3
				HOMO-5→LUMO	-0.4266	36.39
				HOMO-5→LUMO+4	-0.1252	3.13
				HOMO-4→LUMO	0.1092	2.38
				HOMO→LUMO	0.4692	44.02
	0.3117	3.81	325.38	HOMO-6→LUMO	-0.1515	4.5
				HOMO-5→LUMO	0.3630	26.35
				HOMO-5→LUMO+4	0.1064	2.26
				HOMO-4→LUMO	-0.1414	3.99
				HOMO-1→LUMO	-0.2054	8.47
	0.2127	3.92	315.53	HOMO→LUMO	0.4966	49.32
				HOMO-5→LUMO	0.1264	3.19
				HOMO-1→LUMO	0.6642	88.23
				HOMO→LUMO	0.1427	4.07
Triazole functionalized fluorene 67 (acetonitrile)	0.6133	3.67	337.48	HOMO-5→LUMO	0.1188	2.82
				HOMO→LUMO	0.6844	93.68
	0.0993	3.83	323.51	HOMO-6→LUMO	-0.1174	2.75
				HOMO-5→LUMO	0.5197	54.10
				HOMO-5→LUMO+4	0.1422	4.04
				HOMO-1→LUMO	-0.3982	31.71
	0.3619	4.72	262.22	HOMO-3→LUMO	-0.2216	9.82
				HOMO-3→LUMO+1	-0.2195	9.63
				HOMO-1→LUMO+1	0.3712	27.55
				HOMO-1→LUMO+2	-0.1075	2.31
				HOMO-1→LUMO+3	-0.2753	15.15
				HOMO-1→LUMO+5	0.1136	2.58
				HOMO→LUMO+1	-0.3155	19.90
	HOMO→LUMO+3	0.2051	8.41			

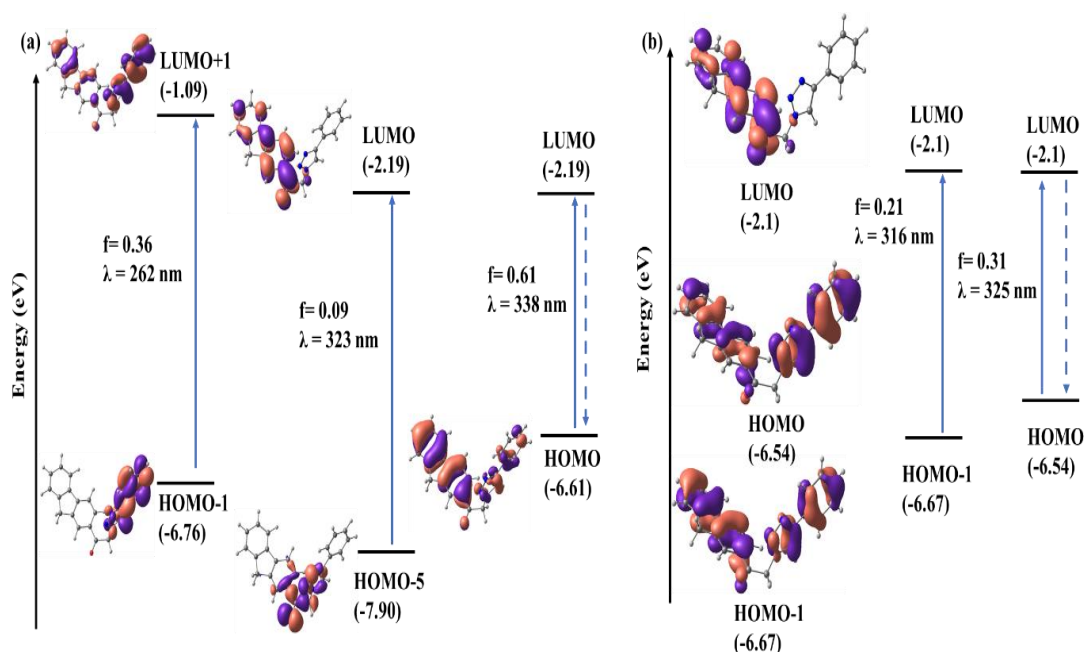


Fig. 36 The important electronic calculations of the triazole functionalized fluorene **67** at M06/Def2-TZVPP //BP86/Def2-SVP level of theory in (a) acetonitrile using the PCM solvent model and (b) gas phase. The corresponding λ in nm and oscillator strength (f) is given. Eigenvalues are given in eV in parentheses.

6.5 *In vitro* antibacterial studies

In vitro antibacterial activity of triazoles (**60a**, **60b**, **60c** and **60d**), triazole functionalised fluorene **67** and thioamide functionalised fluorene **69** against *Bacillus subtilis*, *Staphylococcus aureus*, *Escherichia coli* and *Pseudomonas aeruginosa* were carried out at $30 \mu\text{gdisc}^{-1}$ in DMSO. The disc diffusion method was used for this purpose. The antibacterial activity was expressed in terms of the mean diameter of the zone of inhibition in millimetres. The activity of the synthesised compounds was compared with that of *chloramphenicol* which was selected as the standard antibiotic for the study. The paper disc dipped in DMSO was used as the negative control and that dipped in *chloramphenicol* served as the positive control. The plates were incubated at 37°C for 24h and the zone of inhibition was measured.

6.5.1 *In vitro* antibacterial studies of triazoles

In vitro antibacterial activity of triazoles **60a**, **60b**, **60c** and **60d** against *Bacillus subtilis*, *Staphylococcus aureus*, *Escherichia coli* and *Pseudomonas aeruginosa* was carried out at 30 µgdisc⁻¹ in DMSO. The results of the study are summarised in **Table 6** and in **Fig. 37**.

The diameter of the zone of inhibition exhibited by the triazoles **60a**, **60b**, **60c** and **60d** were compared with that of chloramphenicol and DMSO. It was found that all the triazoles exhibited appreciable antibacterial activity.

Table.6 Antibacterial activity of triazoles **60**:

Sl. No.	Triazole 60	Diameter of zone of inhibition in mm			
		B. subtilis	S. aureus	E.coli	P. aeruginosa
1	60a	12	16	13	10
2	60b	14	18	19	12
3	60c	8	12	7	11
4	60d	9	11	6	10
5	DMSO	Nil	9	Nil	7
6	Chloramphenicol	22	10	20	9

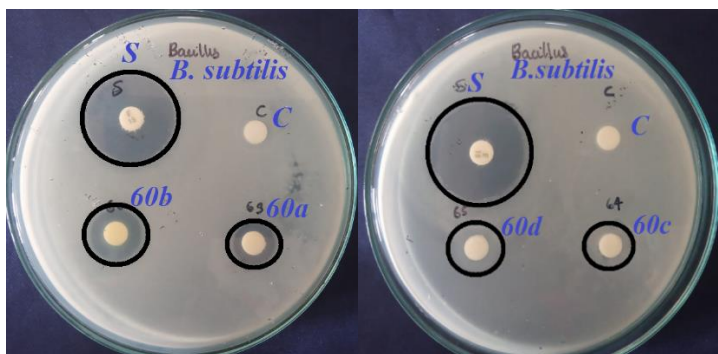


Fig. 37a

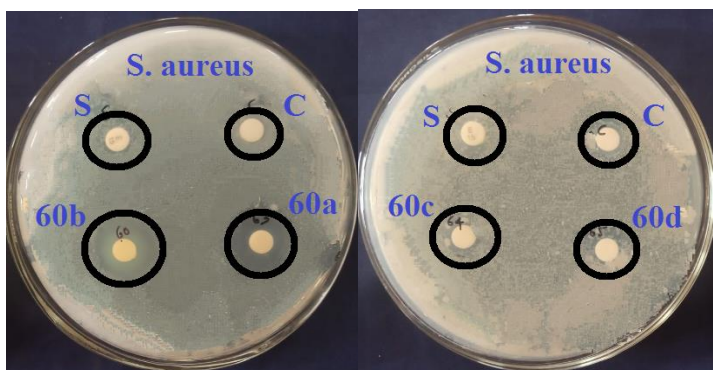


Fig. 37b

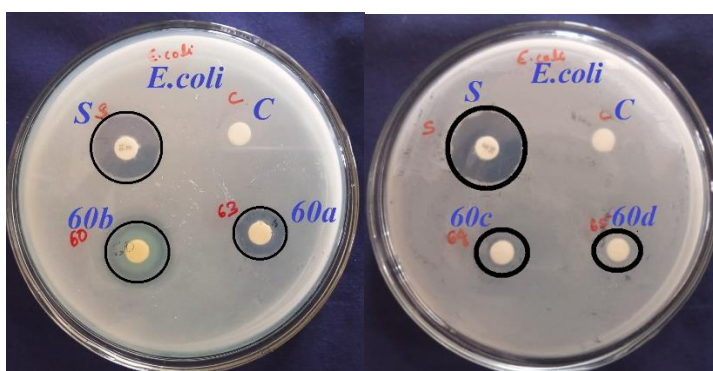


Fig. 37c

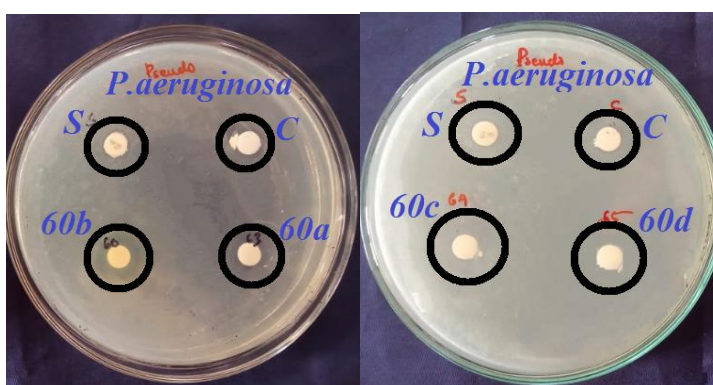


Fig.37d

Fig. 37 Antibacterial activity of compounds 60a, 60b, 60c and 60d against; (37a) *Bacillus subtilis*, (37b) *Staphylococcus aureus*, (37c) *Escherichia coli* and (37d) *Pseudomonas aeruginosa*.

Chapter-6

The zone of inhibition exhibited by the triazoles **60a**, **60b**, **60c** and **60d** against *Bacillus subtilis* was 12 mm, 14 mm, 8 mm and 9 mm respectively. It was also found that chloramphenicol exhibited a zone of inhibition of 22 mm while DMSO exhibited no zone of inhibition. The comparison of the zone of inhibitions showed that the triazoles **60a**, **60b**, **60c** and **60d** are active against *Bacillus subtilis* but the activity of these compounds is less than that of the standard.

The zone of inhibition exhibited by the triazoles **60a**, **60b**, **60c** and **60d** against *Staphylococcus aureus* was 16 mm, 18 mm, 12 mm and 11mm respectively. The zone of inhibition exhibited by the chloramphenicol was 10 mm and that of DMSO was 9 mm. Since the triazoles **60a**, **60b**, **60c** and **60d** exhibited a larger zone of inhibition than the standard compound, it was clear that these compounds possess much better activity against the bacteria *Staphylococcus aureus* than the standard compound. Therefore it can be concluded that these compounds are very effective antibacterial agents against *Staphylococcus aureus*.

The zone of inhibition exhibited by the triazoles **60a**, **60b**, **60c** and **60d** against *Escherichia coli* was 13 mm, 19 mm, 7 mm and 6 mm respectively. It was also found that chloramphenicol exhibited a zone of inhibition of 20 mm while DMSO exhibited no zone of inhibition. The comparison of the zone of inhibitions showed that the triazoles **60a**, **60b**, **60c** and **60d** are active against *Escherichia coli* but the activity of these compounds is less than that of the standard.

The zone of inhibition exhibited by the triazoles **60a**, **60b**, **60c** and **60d** against *Pseudomonas aeruginosa* was 10 mm, 12 mm, 11 mm and 10 mm respectively. It was observed that the chloramphenicol exhibited a zone of inhibition of 9 mm while that of DMSO was 7 mm. The diameter of the zone of inhibitions showed that the triazoles **60a**, **60b**, **60c** and **60d** are better antibacterial agents against *Pseudomonas aeruginosa* than the standard.

6.5.2 In vitro antibacterial studies of fluorene derivatives

In vitro antibacterial activity of fluorene derivatives **67** and **69** against *Bacillus subtilis*, *Staphylococcus aureus*, *Escherichia coli* and *Pseudomonas aeruginosa* were carried out at a concentration of 30 μgdisc^{-1} in DMSO. The results of the study are summarised in **Table 7** and in **Fig. 38**.

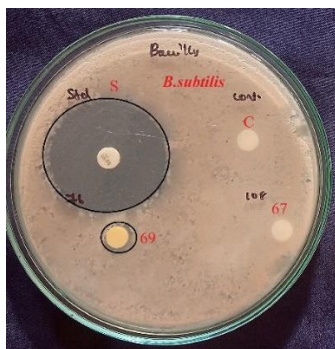


Fig. 38a

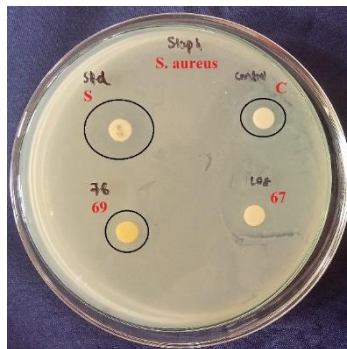


Fig. 38b

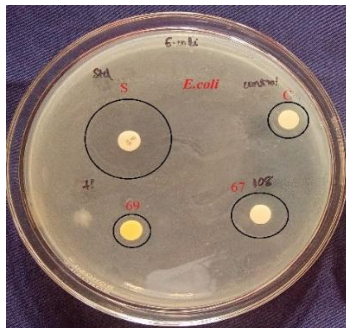


Fig. 38c

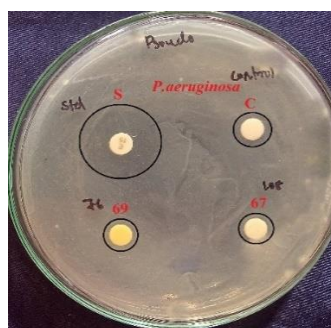


Fig. 38d

Fig. 38 Antibacterial activity of fluorene derivatives **67** and **69** against; (38a) *Bacillus subtilis*, (38b) *Staphylococcus aureus*, (38c) *Escherichia coli* and (38d) *Pseudomonas aeruginosa*.

The zone of inhibitions exhibited by the fluorene derivatives **67** and **69** against *Bacillus subtilis* was 0 mm and 6 mm respectively. It was also found that chloramphenicol exhibited a zone of inhibition of 35 mm while DMSO exhibited no zone of inhibition. A comparison of the zone of inhibitions showed that the triazole

functionalized fluorene **67** is inactive against *Bacillus subtilis*. But the thioamide functionalized fluorene **69** is slightly active against *Bacillus subtilis*.

The zone of inhibitions exhibited by the fluorene derivatives **67** and **69** against *Staphylococcus aureus* was 0 mm and 6 mm respectively. It was also found that chloramphenicol exhibited a zone of inhibition of 17 mm while DMSO exhibited a zone of inhibition of 7 mm. The comparison of the zone of inhibitions showed that the fluorene derivatives **67** and **69** are inactive against *Staphylococcus aureus*.

Table.7 Antibacterial activity of fluorene derivatives **67** and **69**:

Sl. No	Sample	Diameter of zone of inhibition in mm			
		<i>B. subtilis</i>	<i>S. aureus</i>	<i>E.coli</i>	<i>P. aeruginosa</i>
1	67	Nil	Nil	13	6
2	69	6	6	9	8
3	DMSO	Nil	7	10	7
4	Chloramphenicol	35	17	23	19

The zone of inhibitions exhibited by the fluorene derivatives **67** and **69** against *Escherichia coli* was 13 mm and 9 mm respectively. It was also found that chloramphenicol exhibited a zone of inhibition of 23 mm while DMSO exhibited a zone of inhibition of 10 mm. The comparison of the zone of inhibitions showed that the triazole functionalized fluorene **67** is active against *Escherichia coli* but the activity is less than that of the standard. Since the zone of inhibition obtained for the thioamide functionalized fluorene **69** is less than that of the control used, it can be considered as inactive against *Escherichia coli*.

The zone of inhibitions exhibited by the fluorene derivatives **67** and **69** against *Pseudomonas aeruginosa* was 6 mm and 8 mm respectively. It was also found that chloramphenicol exhibited a zone of inhibition of 19 mm while DMSO exhibited a zone of inhibition of 7 mm. The comparison of the zone of inhibitions showed that the triazole functionalized fluorene **67** is inactive against *Pseudomonas aeruginosa*, but the thioamide functionalized fluorene **69** is slightly active against *Pseudomonas aeruginosa*.

6.6 Molecular docking studies on antibacterial activity

The antibacterial activity of the synthesised triazole **60b**, triazole functionalized fluorene **67** and thioamide functionalized fluorene **69** against the proteins; FtsZ and DNA gyrase was theoretically calculated using *in silico* molecular docking methods. The study was performed using the docking programme Autodock vina. The binding modes as well as the binding energy of the triazole **60b**, triazole functionalized fluorene **67** and thioamide functionalized fluorene **69** with the target proteins have been calculated. The interactions between the proteins and the ligand were checked using the Discovery Studio visualizer.

6.6.1 Docking studies on triazole

The *in vitro* antibacterial activity of the triazoles **60a**, **60b**, **60c** and **60d** has been analysed against four bacterial strains; *Bacillus subtilis*, *Staphylococcus aureus*, *Escherichia coli* and *Pseudomonas aeruginosa*. From this study, it was found that the triazole **60b** exhibited better antibacterial activity compared to the other three triazoles and its activity was more prominent against the bacteria *Staphylococcus aureus*. So we decided to theoretically analyse the antibacterial properties of the triazole **60b** against the proteins FtsZ (PDB id: 3vob) and DNA gyrase (PDB id: 2xcs) present in the bacteria *Staphylococcus aureus* (**Fig. 39**) using *in silico* molecular docking methods.

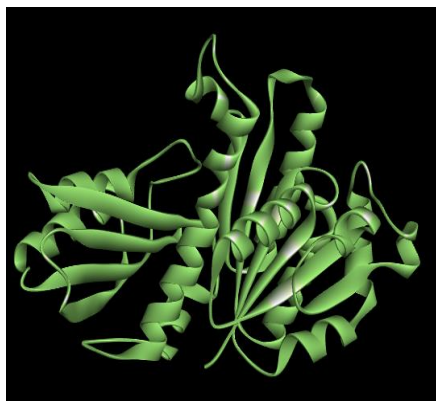


Fig. 39a

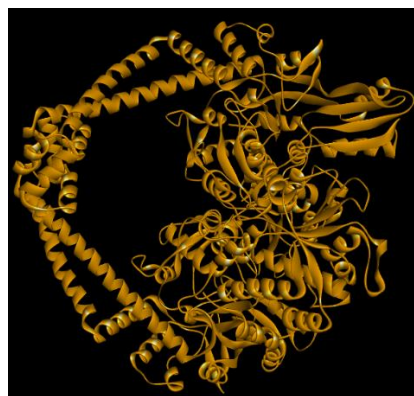


Fig. 39b

Fig. 39. (39a) Structure of *Staphylococcus aureus* FtsZ (PDB id: 3vob)

(39b) Structure of *Staphylococcus aureus* DNA gyrase (PDB id: 2xcs)

The binding modes of the triazole **60b** with the target proteins; FtsZ and DNA gyrase has been analysed (**Fig. 40**). The binding energy and various interactions of the ligand with active site residues of FtsZ and DNA gyrase (**Fig. 41**) are summarised in **Table 8**.

The binding energy of triazole **60b** with the protein FtsZ was -7.0 kcal/mol. The ligand formed a single hydrogen bond interaction with LEU A:200 together with Van der Waals, pi-anion, pi-sigma, amide-pi stacked, alkyl and pi-alkyl interactions.

The binding energy of triazole **60b** with the protein DNA gyrase was -6.8 kcal/mol. The ligand formed a single hydrogen bond interaction with SER B:1098 together with Van der Waals, pi-pi T-shaped, alkyl and pi-alkyl interactions.

The binding energy values showed that triazole **60b** is a good inhibitor for the proteins; FtsZ and DNA gyrase. The highest binding energy was obtained for the ligand **60b** with the protein, FtsZ which showed that triazole **60b** is a better inhibitor for FtsZ than DNA gyrase. The values obtained in the docking study established that triazole **60b** exhibit good antibacterial properties.

Table. 8 Binding energies and possible interactions of triazole **60b** with proteins:

Ligand	Protein	Binding energy (Kcal/mol)	H-bonds	Other interactions
Triazole (60b)	<i>S. aureus</i> FtsZ (PDB id: 3vob)	-7.0	LEU A:200	Van der Waals Pi-anion Pi-sigma Amide-Pi stacked alkyl Pi-alkyl
	<i>S. aureus</i> DNA gyrase (PDB id: 2xcs)	-6.8	SER B:1098	Van der Waals Pi-Pi T-shaped Alkyl Pi-alkyl

Fig. 40a



Fig. 40b



Fig. 40. (40a) Bound conformation of *Staphylococcus aureus* FtsZ and triazole 60b
(40b) Bound conformation of *Staphylococcus aureus* DNA gyrase and triazole 60b

Fig. 41a

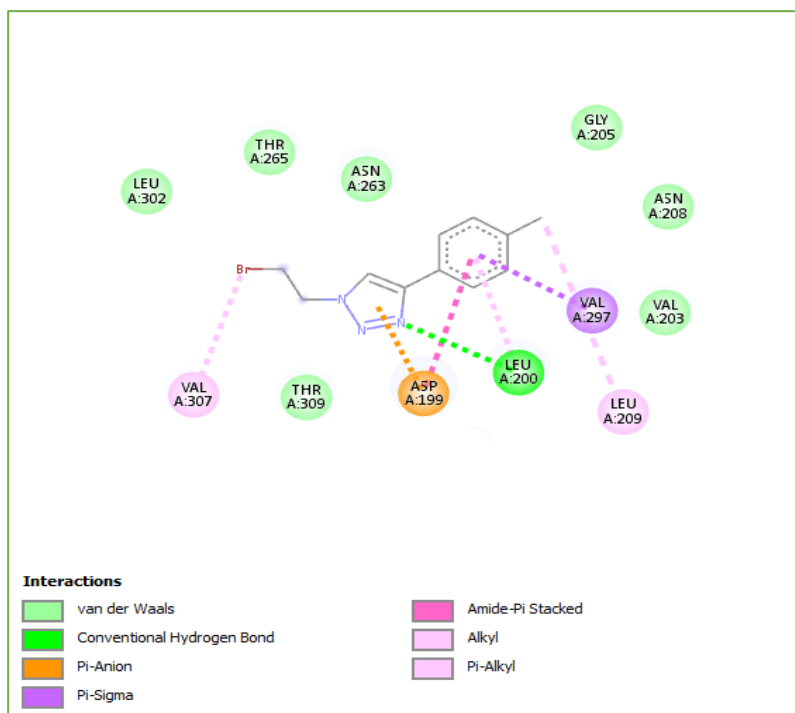


Fig. 41b

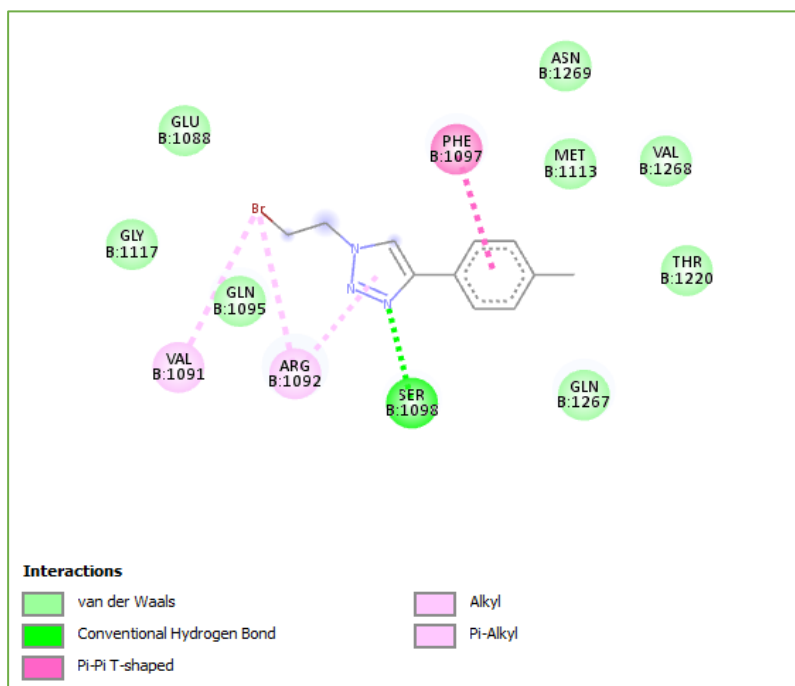


Fig. 41. (41a) Interaction between *Staphylococcus aureus* FtsZ and triazole **60b**
 (41b) Interaction between *Staphylococcus aureus* DNA gyrase and triazole **60b**

6.6.2 Docking studies on triazole functionalized fluorene

The *in vitro* antibacterial activity of the triazoles functionalized fluorene **67** has been analysed against four bacterial strains; *Bacillus subtilis*, *Staphylococcus aureus*, *Escherichia coli* and *Pseudomonas aeruginosa*. From this study, it was found that the triazoles functionalized fluorene **67** is most effective against the bacteria *Escherichia coli*. So we decided to theoretically analyse the antibacterial properties of the triazoles functionalized fluorene **67** against the proteins FtsZ (PDB id: 6LL6) and DNA gyrase present in the bacteria *Escherichia coli* (**Fig. 42**) using *in silico* molecular docking methods.



Fig. 42a

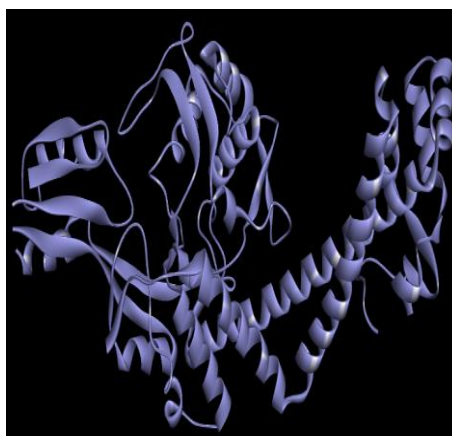


Fig. 42b

Fig. 42. (42a) Structure of *Escherichia coli* FtsZ (PDB id: 6LL6); (42b) Structure of *Escherichia coli* DNA gyrase (PDB id: 1AB4)

The binding modes of the triazoles functionalized fluorene **67** with the target proteins; FtsZ and DNA gyrase has been analysed (**Fig. 43**). The binding energy and various interactions of the ligand with active site residues of FtsZ and DNA gyrase (**Fig. 44**) are summarised in **Table 9**.

The binding energy of the triazoles functionalized fluorene **67** with the protein FtsZ was -8.1 kcal/mol. The ligand formed two hydrogen bond interactions with THR A:309 and SER A:227 together with Van der Waals interactions, carbon-hydrogen bond, pi-donor hydrogen bond, pi-sulfur and pi-alkyl interactions.

The binding energy of the triazoles functionalized fluorene **67** with the protein DNA gyrase was -8.4 kcal/mol. There is no hydrogen bond interaction between ligand and protein. The interactions between the ligand and protein include Van der Waals interactions, pi-anion, pi-pi stacked and pi-alkyl interactions.

The binding energy values showed that the triazoles functionalized fluorene **67** is a good inhibitor for the proteins; FtsZ and DNA gyrase. The greater binding energy was obtained for the triazoles functionalized fluorene **67** with the protein, DNA gyrase which showed that the triazoles functionalized fluorene **67** is a better inhibitor for DNA gyrase than FtsZ. The values obtained in the docking study established that the triazoles functionalized fluorene **67** exhibits good antibacterial properties.

Table. 9 Binding energies and possible interactions of the triazoles functionalized fluorene **67** with proteins:

Ligand	Protein	Binding energy (Kcal/mol)	H-bonds	Other interactions
Compound (67)	<i>E. coli</i> FtsZ (PDB id: 6LL6)	-8.1	THR A:309 SER A:227	Van der Waals C-H bond Pi-donor H-bond Pi-sulfur Pi-alkyl
	<i>E. coli</i> DNA gyrase (PDB id: 1AB4)	-8.4	Nil	Van der Waals Pi-anion Pi-Pi stacked Pi-alkyl

Fig. 43a



Fig. 43b

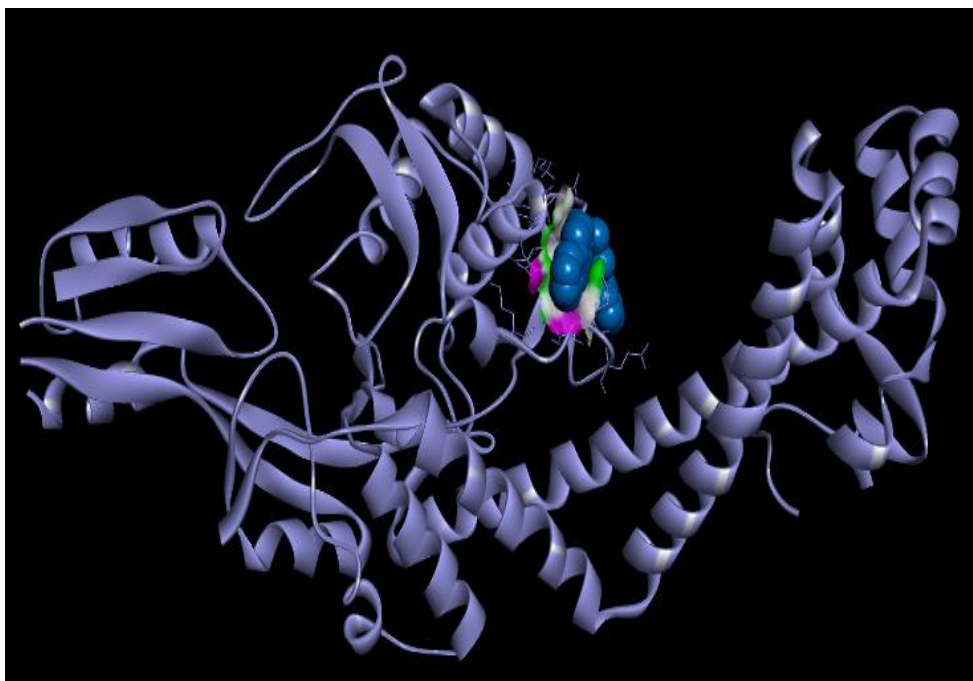


Fig. 43. (43a) Bound conformation of *Escherichia coli* FtsZ and ligand **67**
(43b) Bound conformation of *Escherichia coli* DNA gyrase and ligand **67**

Fig. 44a

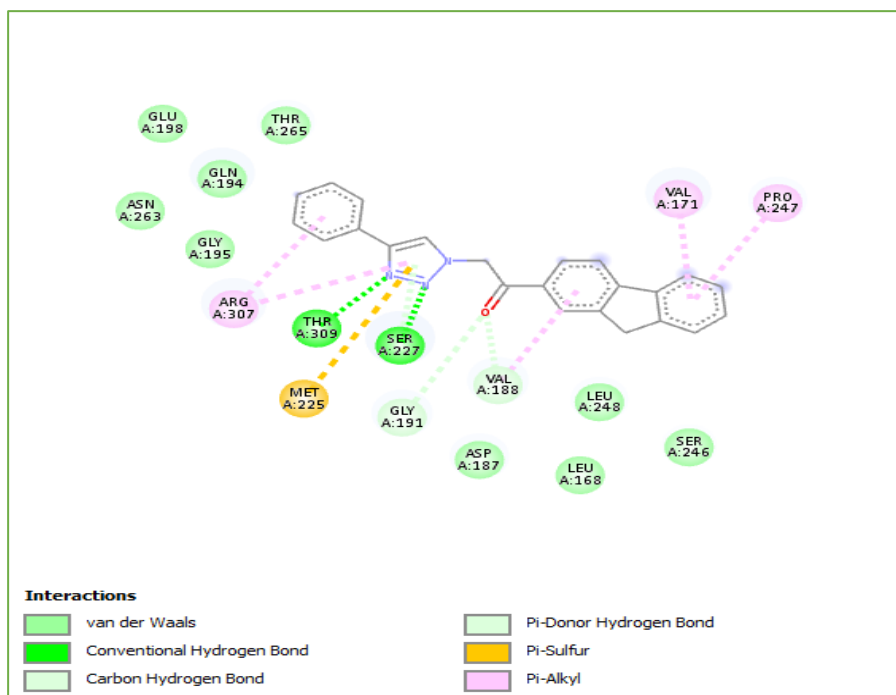


Fig. 44b

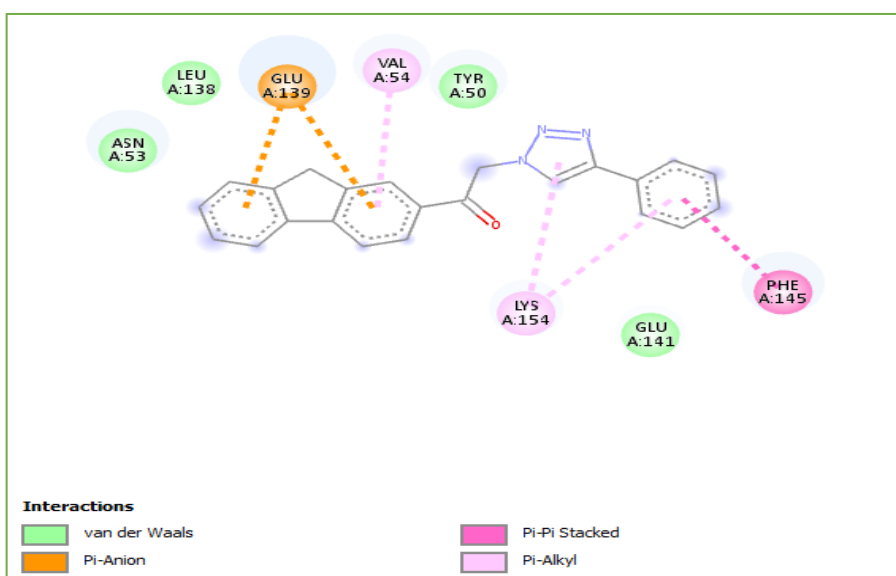


Fig. 44. (44a) Interaction between *Escherichia coli* FtsZ and ligand 67

(44b) Interaction between *Escherichia coli* DNA gyrase and ligand 67

6.6.3 Docking studies on thioamide functionalized fluorene

The *in vitro* antibacterial activity of the thioamide functionalized fluorene **69** has been analysed against four bacterial strains; *Bacillus subtilis*, *Staphylococcus aureus*, *Escherichia coli* and *Pseudomonas aeruginosa*. From this study, it was found that the thioamide functionalized fluorene **69** is most effective against the bacteria *Pseudomonas aeruginosa*. So we decided to theoretically analyse the antibacterial properties of the thioamide functionalized fluorene **69** against the proteins FtsZ (PDB id: 2VAW) and DNA gyrase (PDB id: AF-P48372) present in the bacteria *Pseudomonas aeruginosa* (**Fig. 45**) using *in silico* molecular docking methods.

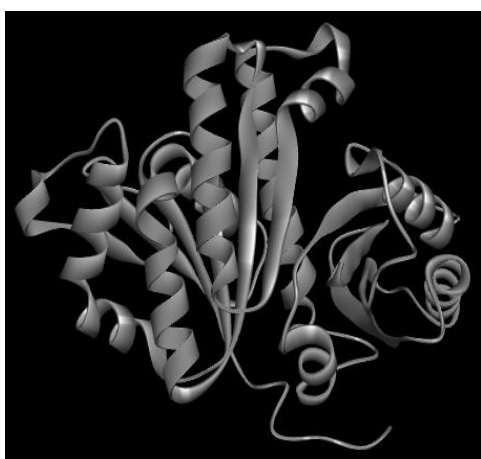


Fig. 45a

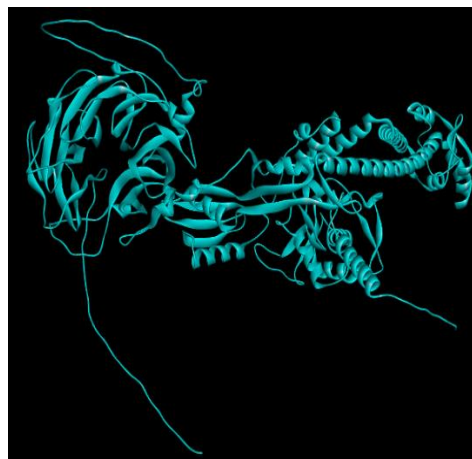


Fig. 45b

Fig. 45. (45a) Structure of *Pseudomonas aeruginosa* FtsZ (PDB id: 2VAW)

(45b) Structure of *Pseudomonas aeruginosa* DNA gyrase (PDB id: AF-P48372)

The binding modes of the thioamide functionalized fluorene **69** with the target proteins; FtsZ and DNA gyrase has been analysed (**Fig. 46**). The binding energy and various interactions of the ligand with active site residues of FtsZ and DNA gyrase (**Fig. 47**) are summarised in **Table 10**.

The binding energy of the thioamide functionalized fluorene **69** with the protein FtsZ was -6.5 kcal/mol. There is no hydrogen bond interaction between ligand and protein. The interactions between the ligand and protein include Van der Waals interactions, pi-donor hydrogen bond, pi-sigma, pi-pi T-shaped and pi-alkyl interactions.

The binding energy of the thioamide functionalized fluorene **69** with the protein DNA gyrase was -6.6 kcal/mol. The ligand formed one hydrogen bond interaction with GLU A:881 together with Van der Waals interactions, carbon-hydrogen bond, pi-sigma and pi-alkyl interactions.

The binding energy values showed that thioamide functionalized fluorene **69** is a good inhibitor for the proteins; FtsZ and DNA gyrase. The greater binding energy was obtained for the thioamide functionalized fluorene **69** with the protein, DNA gyrase which showed that the thioamide functionalized fluorene **69** is a better inhibitor for DNA gyrase than FtsZ. The values obtained in the docking study established that the thioamide functionalized fluorene **69** exhibits good antibacterial properties.

Table. 10 Binding energies and possible interactions of the thioamide functionalized fluorene **69** with proteins:

Ligand	Protein	Binding energy (Kcal/mol)	H-bonds	Other interactions
Compound (69)	<i>P. aeruginosa</i> FtsZ (PDB id: 2VAW)	-6.5	NIL	Van der Waals Pi-donor H-bond Pi-sigma Pi-pi T-shaped Pi-alkyl
	<i>P. aeruginosa</i> DNA gyrase (PDB id: AF-P48372)	-6.6	GLU A:881	Van der Waals C-H bond Pi-sigma Pi-alkyl

Fig. 46a

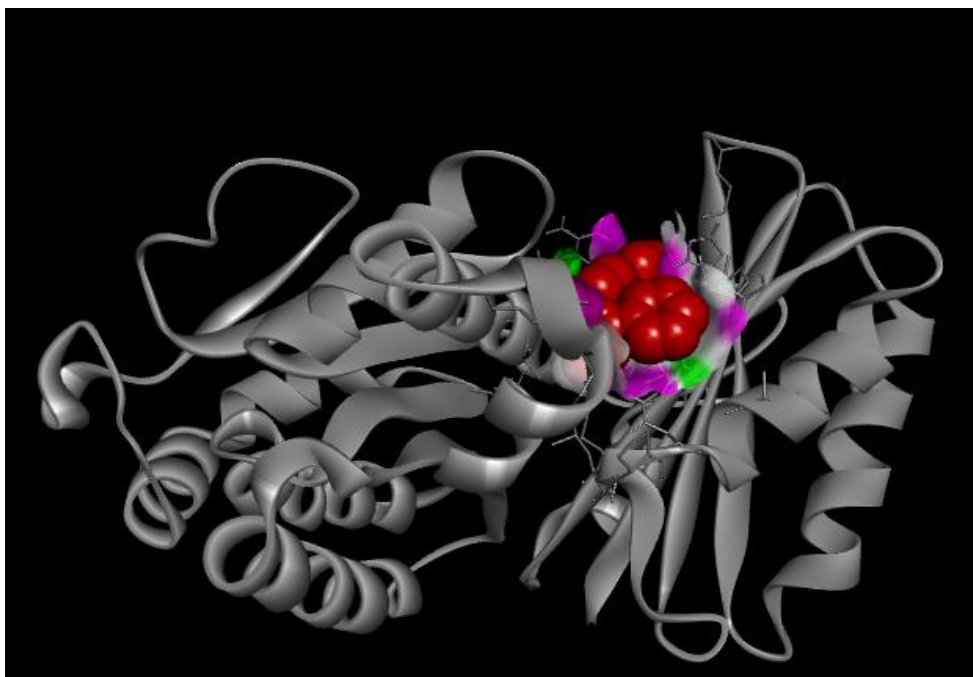


Fig. 46b



Fig. 46. (46a) Bound conformation of *Pseudomonas aeruginosa* FtsZ and ligand **69**
(46b) Bound conformation of *Pseudomonas aeruginosa* DNA gyrase and ligand **69**

Fig. 47a

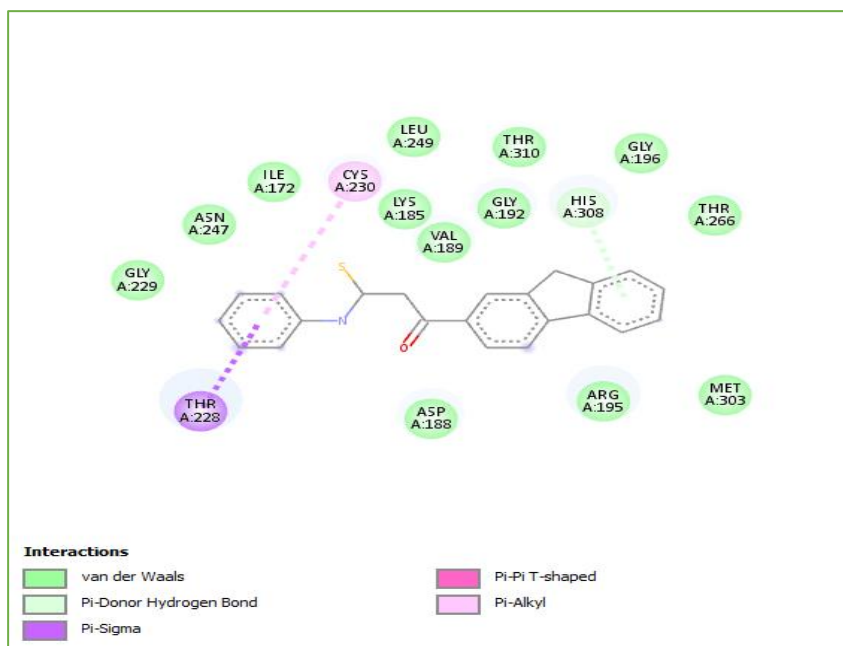


Fig. 47b

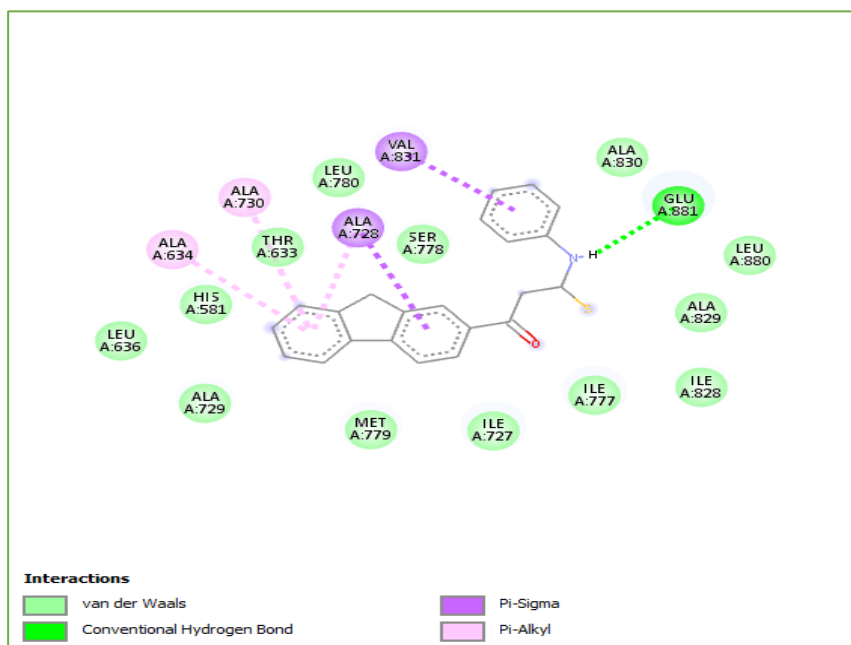


Fig. 47. (47a) Interaction between *Pseudomonas aeruginosa* FtsZ and ligand **69**
 (47b) Interaction between *Pseudomonas aeruginosa* DNA gyrase and ligand **69**

6.7 Experimental details

6.7.1 Materials and methods

All the chemicals used for the synthesis were purchased from Sigma-Aldrich, Bangalore, India. Organic solvents were purchased from Spectrochem, India. Solvents were used without further purification. FT-IR spectra were recorded on Perkin Elmer Spectrum Two FT-IR with a wavelength range of 8300-350 cm^{-1} and spectral resolution of 0.5 cm^{-1} . ^1H NMR spectra were recorded at 400 MHz and ^{13}C NMR spectra were recorded at 100 MHz on a Bruker Avance III NMR spectrometer (Germany). Chemical shifts are quoted in parts per million (ppm) relative to TMS ($\delta=0$) as the internal standard in CDCl_3 . The abbreviations used are as follows: s, singlet; d, doublet; m, multiplet. Coupling constant (J) values are given in hertz (Hz). Reactions were monitored by thin-layer chromatography (TLC) using TLC sheets coated with UV fluorescent silica gel Merck 60 F254 plates and were visualized using a UV lamp. Chromatography was carried out using silica gel 60-120 mesh (Merck, India) and different solvents as mobile phases.

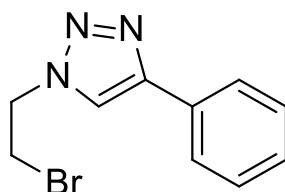
UV-Visible spectral analysis was carried out on Shimadzu UV-1800 Spectrometer. Spectrofluorometric studies were recorded on a Jasco Spectrofluorometer having a shielded lamp house of 150 W Xe lamp. The wavelength range of the spectrofluorometer was 200-900 nm and wavelength accuracy was ± 2 nm. Molecular docking studies were performed with the help of Green Clones Naturals Pvt. Ltd., Ernakulam.

6.7.2 Synthesis of triazoles

A 100 mL RB flask equipped with magnetic bead was charged with 1,2-dihaloethane **57** (18 mmol, 4 eq.), alkyne **58** (5 mmol, 1 eq.) and sodium azide **59** (7 mmol, 1.5 eq.). To this reaction mixture, copper supported polymer catalyst (CuPVPNNMBA) (10 mg) was added as the catalyst. A mixture of distilled water (3 mL) and t-butyl alcohol (9 mL) was added as the solvent. The reactants were stirred at room temperature for 30 min. and gradually increased the temperature to 60 $^\circ\text{C}$. The reaction proceeded smoothly giving triazoles **60** in good yields within 24h. After the completion of the reaction (monitored by TLC), the reaction mixture was

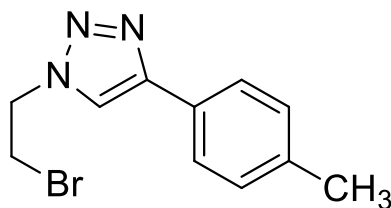
diluted with water (50 mL), extracted with chloroform (3 x 20 mL) and dried over anhydrous sodium sulphate. The solvent was removed by evaporation and the product was purified using silica gel column chromatography using hexane: chloroform (1:1) as eluent to afford triazole **60**.

(a) *1-(2-bromoethyl)-4-phenyl-1H-1,2,3-triazole(60a)*

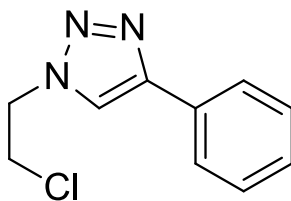


^1H NMR (400 MHz, CDCl_3): δ 7.84 (s, 1H), 7.37-7.27 (m, 2H), 7.77-7.75 (m, 2H), 7.26-7.24 (m, 1H), 4.71 (t, $J = 4.6$, 2H), 3.71 (t, $J = 4.6$, 2H); ^{13}C NMR (100 MHz, CDCl_3): δ 146.4, 129.0, 127.7, 127.2, 124.6, 119.5, 50.5, 28.3; FT-IR (KBr): 3049, 2114, 1732, 1452, 1220, 1078, 838, 766, 686, 630 and 518 cm^{-1} .

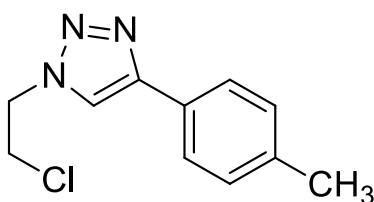
(b) *1-(2-bromoethyl)-4-(p-tolyl)-1H-1,2,3-triazole (60b)*



^1H NMR (400 MHz, CDCl_3): δ 7.78 (s, 1H), 7.67 - 7.65 (m, 2H), 7.19 - 7.16 (m, 2H), 4.73 (t, $J = 4.6$, 2H), 3.73 (t, $J = 4.6$, 2H), 2.31 (s, 3H); ^{13}C NMR (100 MHz, CDCl_3): δ 147.8, 138.2, 129.5, 127.4, 125.7, 120.1, 51.6, 29.7, 21.3; FT-IR (KBr): 3407, 2106, 1716, 1452, 1228, 1014, 806, 726, 670 and 526 cm^{-1} .

(c) *1-(2-chloroethyl)-4-phenyl-1H-1,2,3-triazole(60c)*

^1H NMR (400 MHz, CDCl_3): δ 7.83 (s, 1H), 7.77 - 7.74 (m, 2H), 7.37 - 7.33 (m, 2H), 4.64 (t, $J=4.3$, 2H), 3.87 (t, $J=4.3$, 2H), 7.28 - 7.24 (m, 1H); ^{13}C NMR (100 MHz, CDCl_3): δ 147.7, 130.3, 128.9, 128.3, 125.7, 120.8, 51.8, 42.5; FT-IR (KBr): 3089, 2106, 1612, 1460, 1212, 1022, 838, 758, 694 and 518 cm^{-1} .

(d) *1-(2-chloroethyl)-4-(p-tolyl)-1H-1,2,3-triazole(60d)*

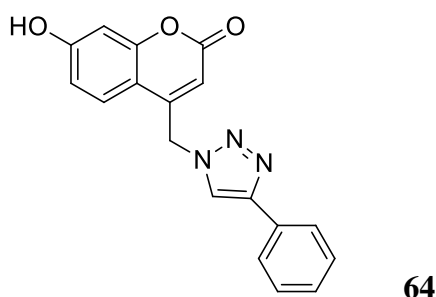
^1H NMR (400 MHz, CDCl_3): δ 7.79 (s, 1H), 7.66 - 7.64 (m, 2H), 7.18 - 7.15 (m, 2H), 4.64 (t, $J = 4.4$, 2H), 3.87 (t, $J = 4.4$, 2H), 2.30 (s, 3H); ^{13}C NMR (100 MHz, CDCl_3): δ 147.8, 138.2, 129.5, 127.4, 125.7, 120.4, 51.8, 42.5, 21.3; FT-IR (KBr): 3033, 2977, 1732, 1444, 1220, 1038, 814, 734, 662 and 518 cm^{-1} .

6.7.3 Synthesis of triazole functionalized coumarin

(i) Resorcinol **61** (10 mmol, 1 eq.) taken in a 100 mL RB flask was dissolved in conc. H_2SO_4 (20 mL) at $0\text{ }^\circ\text{C}$. Ethyl-4-chloroacetoacetate **62** (10 mmol, 1 eq.) was slowly added to the reaction mixture while stirring. The reaction temperature was slowly increased from $0\text{ }^\circ\text{C}$ to room temperature. The stirring continued for 24h. After the completion of the reaction (monitored by TLC), the reaction mixture was

added to ice water (50 mL) and the 4(chloromethyl)-7-hydroxy-2H-chromene-2-one **63** obtained was collected by filtration through Whatman no.1 filter paper and dried.

(ii) A 100 mL dry RB flask equipped with magnetic bead was charged with 4(chloromethyl)-7-hydroxy-2H-chromene-2-one **63** (1 mmol, 1 eq.), phenylacetylene **58a** (1 mmol, 1 eq.) and sodium azide **59** (1.3 mmol, 1.5 eq.). To this reaction mixture, copper supported polymer catalyst (CuPVPNNMBA) (10 mg) was added. A mixture of distilled water (3 mL) and t-butyl alcohol (9 mL) was added as the solvent. The reactants were stirred at room temperature for 30 min. and gradually increased the temperature to 60 °C. The reaction proceeded smoothly giving triazole functionalized coumarin **64** in good yields within 24h. After the completion of the reaction (monitored by TLC), the reaction mixture was diluted with water (50 mL), extracted with chloroform (3 x 20 mL) and dried over anhydrous sodium sulphate. The chloroform was removed by evaporation using rotavapor. The product was purified by silica gel column chromatography using hexane: chloroform (1:1) as eluent to afford triazole functionalized coumarin **64**.

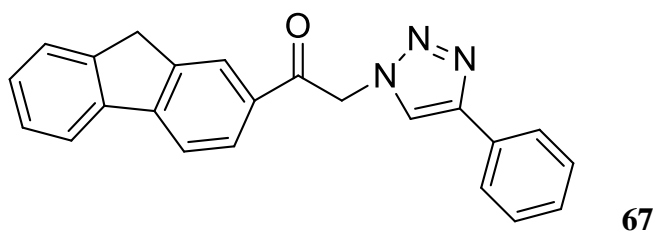


Yield = 84%, mp = 195 °C, ¹H NMR (400 MHz, CDCl₃): δ 9.08 (s, 1H), δ 8.05 (s, 1H), δ 6.25 (s, 1H), δ 4.5 (s, 2H), δ 6.21-6.71 (m, 6H), δ 7.42-7.47 (m, 6H); ¹³C NMR (100 MHz, CDCl₃): δ 161.5, 152.8, 141.4, 134.9, 132.8, 129.9, 128.8, 126.4, 124.2, 122.9, 116.4, 115, 52.1; FT-IR (KBr): 2916, 1711, 1620, 1339, 1102 cm⁻¹.

6.7.4 Synthesis of triazole functionalized fluorene

(i) A 100 mL dry RB flask equipped with a magnetic bead was charged with 2-acetylfluorene **65** (2.4 mmol, 1 eq.) and acetic acid (2 mL). The reaction mixture was heated at a temperature of 65 °C for 10 min to dissolve 2-acetylfluorene in acetic acid. The solution was cooled in an ice bath and to this ice cold solution, bromine (2.4 mmol, 1 eq.) was added and stirred again for 1h at room temperature. After the completion of the reaction (monitored by TLC) the reaction mixture was diluted with distilled water (50 mL) and the 2-(bromoacetyl)fluorene **66** obtained was collected by filtration through Whatman no.1 filter paper and dried.

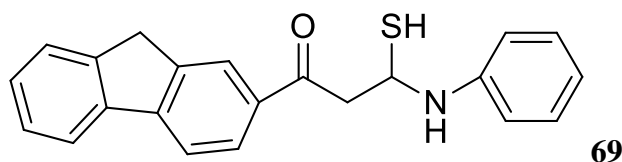
(ii) A 100 mL dry RB flask provided with magnetic bead and guard tube was charged with 2-(bromoacetyl)fluorene **66** (1.7 mmol, 1 eq.), Phenylacetylene **58a** (1.7 mmol, 1 eq.) and sodium azide **59** (1.7 mmol, 1 eq.). To this reaction mixture, copper supported polymer catalyst (CuPVPNNMBA) (10 mg) was added. A mixture of distilled water (3 mL) and t-butyl alcohol (9 mL) was added as the solvent. The reactants were stirred at room temperature for 30 min. and gradually increased the temperature to 60 °C. The reaction proceeded smoothly giving triazole functionalized fluorene **67** in good yields within 24h. After the completion of the reaction (monitored by TLC) the reaction mixture was diluted with distilled water (50 mL) and the product **67** obtained was collected by filtration through Whatman no.1 filter paper and dried.



Yield = 82%, mp = 90 °C, ¹H NMR (400 MHz, CDCl₃): δ 8.12 (s, 1H), δ 7.99 (s, 1H), δ 7.70 (m, 2H), δ 7.39 (s, 1H), δ 7.26 (s, 1H), δ 3.92 (s, 2H), δ 2.65 (s, 2H); ¹³C NMR (100MHz, CDCl₃): δ 197.8, 146.3, 145.3, 142.9, 139.4, 135.9, 130.3, 128.5, 128.0, 127.9, 127.7, 127.0, 125.2, 124.9, 122.0, 120.8, 119.7, 36.7, 26.7; FT-IR (KBr): 2926, 1720, 1464, 1264, 1217, 1671, 1608, 809, 753, 697, 601, 409 cm⁻¹; GCMSMS: *m/z* 351.4 (M⁺).

6.7.5 Synthesis of thioamide functionalized fluorene

A 100 mL ice cold dry RB equipped with a guard tube and magnetic bead was charged with 2-acetylfluorene **65** (1 mmol, 1 eq.), phenyl isothiocyanate **68** (1 mmol, 1 eq.), sodium hydride (2 mmol, 1.7 eq.) and N, N-dimethylformamide (DMF) (8 mL). The reaction mixture was stirred at room temperature for 24h. After the completion of the reaction (monitored by TLC), the reaction mixture was diluted with water (50 mL), extracted with ethyl acetate (3 x 20 mL) and dried over anhydrous sodium sulphate. Ethyl acetate was removed by evaporation using rotavapor. The product was purified using silica gel column chromatography using hexane: ethylacetate (4:1) as eluent to afford thioamide functionalized fluorene **69** as crystals of pale yellow colour.



Yield = 80%, mp = 110 °C, ^1H NMR (400 MHz, CDCl_3): δ 8.20 (d, $J=1.2$ Hz, 1H), δ 8.171 (d, $J=1.6$ Hz, 1H), δ 8.15 (d, $J=1.6$ Hz, 1H), δ 7.73 (s, 1H), δ 7.71 (s, 1H), δ 7.644-7.607 (m, 2H), δ 7.572 (d, $J=0.8$ Hz, 1H), δ 7.55 (d, $J=0.8$ Hz, 1H), δ 7.53 (d, $J=0.8$ Hz, 1H), δ 7.40 (d, $J=0.8$ Hz, 1H), δ 7.38 (d, $J=0.8$ Hz, 1H), δ 5.7 (s, 1H), δ 4.1 (s, 1H), δ 2.7 (s, 2H), δ 2.636 (s, 2H), δ 1.2 (s, 1H); ^{13}C NMR (100MHz, CDCl_3): δ 196.5, 148.4, 143.2, 137.8, 135.0, 134.8, 134.3, 130.2, 124.6, 124.1, 121.2, 120.4, 60.8, 30.9, 26.6; FTIR (KBr): 2934, 2846, 1703, 1671, 1616, 1256, 1192, 1120, 977, 848, 753,745, 681, 609 cm^{-1} ; GCMSMS: m/z 345.5 (M^+).

6.8 Conclusion

Thorium is widely used in nuclear power generators and in the preparation of alloys and nuclear medicine. Although it finds various applications, it is very dangerous to the ecosystem. It is highly carcinogenic and also causes mutation in living organisms. Therefore monitoring thorium contamination in the environment is very essential. Various techniques such as gravimetric analysis,

Chapter-6

chromatographic techniques, titrimetry, electro-analytical techniques and fluorimetry have been developed for the detection and estimation of thorium. But, these techniques are highly expensive and require sophisticated instruments. Here comes the importance of fluorescent sensors which is a low-cost, highly sensitive and selective technique for the detection of metal ions.

Triazoles as well as fluorene derivatives exhibit fluorescence. The intensity of fluorescence enhances upon complexation with thorium. Therefore, triazoles are used as chemosensors for the detection of thorium ions. In our work, we have devised new synthetic strategies for triazoles and fluorene derivatives that can be used as fluorescent sensors for thorium (IV) ions. The characterisation of the synthesised compounds was performed using FT-IR, ^1H NMR, ^{13}C NMR and GCMSMS.

The triazoles (**60a**, **60b**, **60c** and **60d**), triazole functionalized coumarin **64**, triazole functionalized fluorene **67** and thioamide functionalized fluorene **69** exhibit fluorescence. The intensity of fluorescence increases upon complexation with thorium (IV) ion for all the compounds except triazole functionalized coumarin **64**. A fluorescence quenching was observed in the case of triazole functionalized coumarin **64** upon complexation with Th^{4+} ion. The fluorescence properties of the compounds were studied with the help of a UV cabinet, UV-visible spectrometer and spectrofluorometer. The change in fluorescence upon complexation with thorium (IV) ion was more prominent in the case of triazole functionalized fluorine **67**. This compound exhibit a shift of fluorescence from UV to the visible range when complexed with Th^{4+} ion. This property makes it an efficient detector for Th^{4+} ions even at the micromolar levels.

In vitro antibacterial activity of the triazoles (**60a**, **60b**, **60c** and **60d**), triazole functionalized fluorene **67** and thioamide functionalized fluorene **69** against *Bacillus subtilis*, *Staphylococcus aureus*, *Escherichia coli* and *Pseudomonas aeruginosa* were carried out. The triazoles **60a**, **60b**, **60c** and **60d** were found to be effective antibacterial agents against all four bacteria. The triazole functionalized fluorene **67** was active against *Escherichia coli* but inactive against *Bacillus subtilis*, *Staphylococcus aureus* and *Pseudomonas aeruginosa*. The thioamide functionalized

fluorene **69** was slightly active against *Bacillus subtilis* and *Pseudomonas aeruginosa* but inactive against *Staphylococcus aureus* and *Escherichia coli*.

In silico molecular docking studies of the triazole **60b**, triazole functionalized fluorene **67** and thioamide functionalized fluorene **69** were carried out using the software Autodock vina. The target proteins selected were Ftsz and DNA gyrase. The docking studies proved that these compounds are good antibacterial agents.

References

- (1) Thanakit, P.; Limthin, D.; Leepheng, P.; Suramitr, S.; Phromyothin, D. Functionalized Magnetic Nanoparticles as Chemosensors Based on Fluorene Derivative for Cd(II) Ions Detection. *Ferroelectrics* **2019**, *552*, 108–120. <https://doi.org/10.1080/00150193.2019.1653087>.
- (2) dos Santos Carlos, F.; Nunes, M. C.; De Boni, L.; Machado, G. S.; Nunes, F. S. A Novel Fluorene-Derivative Schiff-Base Fluorescent Sensor for Copper(II) in Organic Media. *J. Photochem. Photobiol. A Chem.* **2017**, *348*, 41–46. <https://doi.org/10.1016/j.jphotochem.2017.08.022>.
- (3) Yi, F. Y.; Chen, D.; Wu, M. K.; Han, L.; Jiang, H. L. Chemical Sensors Based on Metal–Organic Frameworks. *Chempluschem* **2016**, *81*, 1–17. <https://doi.org/10.1002/cplu.201600137>.
- (4) Abbel, R.; Schenning, A. P. H. J.; Meijer, E. W. Fluorene-Based Materials and Their Supramolecular Properties. *J. Polym. Sci. Part A Polym. Chem.* **2009**, *47*, 4215–4233. <https://doi.org/https://doi.org/10.1002/pola.23499>.
- (5) Wong, W. Y. Metallated Molecular Materials of Fluorene Derivatives and Their Analogues. *Coord. Chem. Rev.* **2005**, *249*, 971–997. <https://doi.org/10.1016/j.ccr.2004.10.007>.
- (6) Khaokeaw, C.; Sukwattanasinitt, M.; Rashatasakhon, P. Salicylyl Fluorene Derivatives as Fluorescent Sensors for Cu(II) Ions. *J. Fluoresc.* **2016**, *26*, 745–752. <https://doi.org/10.1007/s10895-016-1766-7>.
- (7) Wang, Z.; Xing, Y.; Shao, H.; Lu, P.; Weber, W. P. Synthesis and Characterization of 9-(Cycloheptatrienylydene)Fluorene Derivatives: Acid-Triggered “Switch on” of Fluorophores. *Org. Lett.* **2005**, *7*, 87–90. <https://doi.org/10.1021/ol047847a>.
- (8) Sil, A.; Islam, S. N.; Patra, S. K. Terpyridyl Appended Poly(Metaphenylene-Alt-Fluorene) II-Conjugated Fluorescent Polymers: Highly Selective and Sensitive Turn off Probes for the Detection of Cu²⁺. *Sensors Actuators, B Chem.* **2018**, *254*, 618–628. <https://doi.org/10.1016/j.snb.2017.07.067>.
- (9) Yi, C.; Song, B.; Tian, W.; Cui, X.; Qi, Q.; Jiang, W.; Qi, Z.; Sun, Y. Fluorescent Sensor of Fluorene Derivatives Having Phosphonic Acid as a Fluorogenic Ionophore: Synthesis and Static Quenched Properties for Fe(III). *Tetrahedron Lett.* **2014**, *55*, 5119–5123. <https://doi.org/10.1016/j.tetlet.2014.05.105>.
- (10) Qian, J.; Lu, Q.; Xu, F.; Chen, L.; Xia, J. Two-Dimensional Nano-Layered Materials as Multi-Responsive Chemosensors Constructed by Carbazole- and Fluorene-Based Polyaniline-like Derivatives. *J. Hazard. Mater.* **2020**, 124544. <https://doi.org/https://doi.org/10.1016/j.jhazmat.2020.124544>.
- (11) Belfield, K. D.; Bondar, M. V; Frazer, A.; Morales, A. R.; Kachkovsky, O. D.; Mikhailov, I. A.; Masunov, A. E.; Przhonska, O. V. Fluorene-Based Metal-Ion Sensing Probe with High Sensitivity to Zn²⁺ and Efficient Two-Photon Absorption. *J. Phys. Chem. B* **2010**, *114*, 9313–9321. <https://doi.org/10.1021/jp104450m>.

- (12) Min, K. S.; Manivannan, R.; Son, Y. A. Rhodamine-Fluorene Based Dual Channel Probe for the Detection of Hg²⁺ Ions and Its Application in Digital Printing. *Sensors Actuators, B Chem.* **2018**, *261*, 545–552. <https://doi.org/10.1016/j.snb.2018.01.178>.
- (13) Wang, Z.; Li, W.; Lu, P. Acidic-Sensing Property of 9-(Cycloheptatrienylidene)Fluorene by UV-Vis Spectroscopy. *Sensors Actuators, B Chem.* **2004**, *99*, 264–266. <https://doi.org/10.1016/j.snb.2003.11.021>.
- (14) Tao, S.; Peng, Z.; Zhang, X.; Wang, P.; Lee, C. S.; Lee, S. T. Highly Efficient Non-Doped Blue Organic Light-Emitting Diodes Based on Fluorene Derivatives with High Thermal Stability. *Adv. Funct. Mater.* **2005**, *15*, 1716–1721. <https://doi.org/10.1002/adfm.200500067>.
- (15) Omer, K. M.; Ku, S. Y.; Wong, K. T.; Bard, A. J. Green Electrogenerated Chemiluminescence of Highly Fluorescent Benzothiadiazole and Fluorene Derivatives. *J. Am. Chem. Soc.* **2009**, *131*, 10733–10741. <https://doi.org/10.1021/ja904135y>.
- (16) Thomas, S. W.; Joly, G. D.; Swager, T. M. Chemical Sensors Based on Amplifying Fluorescent Conjugated Polymers. *Chem. Rev.* **2007**, *107*, 1339–1386. <https://doi.org/10.1021/cr0501339>.
- (17) Rejithamol, R.; Beena, S.; Nair, A. B.; Santhy, A. Synthesis, Characterization and Photophysical Properties of Benzylidene-Fluorene Derivatives. *Mater. Today Proc.* **2018**, *5*, 17694–17698. <https://doi.org/10.1016/j.matpr.2018.06.090>.
- (18) Belfield, K. D.; Schafer, K. J.; Mourad, W.; Reinhardt, B. A. Synthesis of New Two-Photon Absorbing Fluorene Derivatives via Cu-Mediated Ullmann Condensations. *J. Org. Chem.* **2000**, *65*, 4475–4481. <https://doi.org/10.1021/jo991950+>.
- (19) Belfield, K. D.; Hagan, D. J.; Van Stryland, E. W.; Schafer, K. J.; Negres, R. A. New Two-Photon Absorbing Fluorene Derivatives: Synthesis and Nonlinear Optical Characterization. *Org. Lett.* **1999**, *1*, 1575–1578. <https://doi.org/10.1021/ol9909177>.
- (20) Selvakumar, R.; Ashok Kumar, S. K.; Vijayakrishna, K.; Sivaramakrishna, A.; Brahmmananda Rao, C. V. S.; Sivaraman, N.; Sahoo, S. K. Development of Highly Selective Chemosensor for Thorium Estimation. *Sensors Actuators, B Chem.* **2018**, *255*, 1391–1400. <https://doi.org/10.1016/j.snb.2017.08.131>.
- (21) Wen, J.; Dong, L.; Hu, S.; Li, W.; Li, S.; Wang, X. Fluorogenic Thorium Sensors Based on 2,6-Pyridinedicarboxylic Acid-Substituted Tetraphenylethenes with Aggregation-Induced Emission Characteristics. *Chem. - An Asian J.* **2016**, *11*, 49–53. <https://doi.org/10.1002/asia.201500834>.
- (22) Tayade, K.; Kaur, A.; Tetgure, S.; Chaitanya, G. K.; Singh, N.; Kuwar, A. Fluorogenic Ratiometric Dipodal Optode Containing Imine-Amide Linkages: Exploiting Subtle Thorium (IV) Ion Sensing. *Anal. Chim. Acta* **2014**, *852*, 196–202. <https://doi.org/10.1016/j.aca.2014.09.016>.
- (23) Safavi, A.; Sadeghi, M. Design and Evaluation of a Thorium (IV) Selective Optode. *Anal. Chim. Acta* **2006**, *567*, 184–188. <https://doi.org/10.1016/j.aca.2006.03.027>.
- (24) Pham, T. A.; Xu, J.; Raymond, K. N. A Macrocyclic Chelator with Unprecedented Th⁴⁺ Affinity. *J. Am. Chem. Soc.* **2014**, *136*, 9106–9115. <https://doi.org/10.1021/ja503456r>.
- (25) Bozorov, K.; Zhao, J.; Aisa, H. A. 1,2,3-Triazole-Containing Hybrids as Leads in Medicinal Chemistry: A Recent Overview. *Bioorganic Med. Chem.* **2019**, *27*, 3511–3531. <https://doi.org/10.1016/j.bmc.2019.07.005>.
- (26) Sasidharan, D.; Aji, C. V.; Mathew, P. 1,2,3-Triazolylidene Palladium Complex with Triazole Ligand: Synthesis, Characterization and Application in Suzuki–Miyaura Coupling Reaction in Water. *Polyhedron* **2019**, *157*, 335–340. <https://doi.org/10.1016/j.poly.2018.10.022>.
- (27) Mathew, P.; Sasidharan, D.; Rakesh, N. P. Copper(I) Stabilized on N,N'-Methylene Bis-Acrylamide Crosslinked Polyvinylpyrrolidone: An Efficient Reusable Catalyst for Click Synthesis of 1,2,3-Triazoles in Water. *Appl. Organomet. Chem.* **2020**, *34*, 1–13. <https://doi.org/10.1002/aoc.5642>.
- (28) Putra, B. F. *Analisis Hubungan Modal Sosial Terhadap Keberdayaan Petani Karet*;

- 2016; 3. <https://doi.org/10.1007/7081>.
- (29) Lau, Y. H.; Rutledge, P. J.; Watkinson, M.; Todd, M. H. Chemical Sensors That Incorporate Click-Derived Triazoles. *Chem. Soc. Rev.* **2011**, *40*, 2848–2866. <https://doi.org/10.1039/c0cs00143k>.
- (30) Meisner, Q. J.; Accardo, J. V.; Hu, G.; Clark, R. J.; Jiang, D. E.; Zhu, L. Fluorescence of Hydroxyphenyl-Substituted “Click” Triazoles. *J. Phys. Chem. A* **2018**, *122*, 2956–2973. <https://doi.org/10.1021/acs.jpca.8b00577>.
- (31) Srinivasan, K. K.; Neelima, Y.; Alex, J.; Sreejith, G.; Ciraj, A. M.; Rao, J. V. Synthesis of Novel Furobenzopyrone Derivatives and Evaluation of Their Antimicrobial and Antiinflammatory Activity. *Indian J. Pharm. Sci.* **2007**, *69*, 326.
- (32) Shaikh, M. H.; Subhedar, D. D.; Shingate, B. B.; Kalam Khan, F. A.; Sangshetti, J. N.; Khedkar, V. M.; Nawale, L.; Sarkar, D.; Navale, G. R.; Shinde, S. S. Synthesis, Biological Evaluation and Molecular Docking of Novel Coumarin Incorporated Triazoles as Antitubercular, Antioxidant and Antimicrobial Agents. *Med. Chem. Res.* **2016**, *25*, 790–804. <https://doi.org/10.1007/s00044-016-1519-9>.
- (33) Saldabol, N.; Popelis, Y.; Shatz, V.; Slavinskaya, V. Bromination of 2-Acetyl-5-Methylfuran. *Chem. Heterocycl. Compd.* **1999**, *35*, 161–163. <https://doi.org/10.1007/BF02251701>.
- (34) Lin, W.; Cao, X.; Ding, Y.; Yuan, L.; Long, L. A Highly Selective and Sensitive Fluorescent Probe for Hg²⁺ Imaging in Live Cells Based on a Rhodamine-Thioamide-Alkyne Scaffold. *Chem. Commun.* **2010**, *46*, 3529–3531. <https://doi.org/10.1039/b927373e>.
- (35) Puthiyedath, T.; Bahulayan, D. A Click Derived Triazole-Coumarin Derivative as Fluorescence on-off PET Based Sensor for Ca²⁺ and Fe³⁺ Ions. *Sensors Actuators, B Chem.* **2018**, *272*, 110–117. <https://doi.org/10.1016/j.snb.2018.05.126>.
- (36) Neelambra, A. U.; Govind, C.; Devassia, T. T.; Somashekarappa, G. M.; Karunakaran, V. Direct Evidence of Solvent Polarity Governing the Intramolecular Charge and Energy Transfer: Ultrafast Relaxation Dynamics of Push-Pull Fluorene Derivatives. *Phys. Chem. Chem. Phys.* **2019**, *21*, 11087–11102. <https://doi.org/10.1039/c9cp00796b>.
- (37) Nakahama, T.; Kitagawa, D.; Sotome, H.; Ito, S.; Miyasaka, H.; Kobatake, S. Optical Properties and Solvatofluorochromism of Fluorene Derivatives Bearing: S, S - Dioxidized Thiophene. *Photochem. Photobiol. Sci.* **2016**, *15*, 1254–1263. <https://doi.org/10.1039/c6pp00126b>.
- (38) Belfield, K. D.; Bondar, M. V.; Kachkovsky, O. D.; Przhonska, O. V.; Yao, S. Solvent Effect on the Steady-State Fluorescence Anisotropy of Two-Photon Absorbing Fluorene Derivatives. *J. Lumin.* **2007**, *126*, 14–20. <https://doi.org/10.1016/j.jlumin.2006.04.012>.
- (39) Kotaka, H.; Konishi, G. ichi; Mizuno, K. Synthesis and Photoluminescence Properties of π -Extended Fluorene Derivatives: The First Example of a Fluorescent Solvatochromic Nitro-Group-Containing Dye with a High Fluorescence Quantum Yield. *Tetrahedron Lett.* **2010**, *51*, 181–184. <https://doi.org/10.1016/j.tetlet.2009.10.118>.
- (40) Das, K. R.; Antony, M. J.; Varghese, S. Highly Bluish-White Light Emissive and Redox Active Conjugated Poly-N-Phenyl Anthranilic Acid Polymer Fluoroprobe for Analytical Sensing. *Polymer (Guildf)*. **2019**, *181*, 121747. <https://doi.org/10.1016/j.polymer.2019.121747>.
- (41) Belik, A. V. Computation of Vibrational Spectra of 4-Methylfuroxane and 3-Methylfuroxane Molecules in Coordinates $X \Delta 0$ with an Estimation of a Force Fields in Frameworks DFT. **2016**, *34*, 2015–2016.
- (42) Trisolini, M. G.; Cromwell, J.; Pope, G. C. Conclusions: Planning for Second-Generation Pay for Performance. *Pay Perform. Heal. Care Methods Approaches* **2011**, 341–370. <https://doi.org/10.3768/rtipress.2011.bk.0002.1103.12>.
- (43) Zhao, Y.; Truhlar, D. G. The M06 Suite of Density Functionals for Main Group Thermochemistry, Thermochemical Kinetics, Noncovalent Interactions, Excited

Chapter-6

- States, and Transition Elements: Two New Functionals and Systematic Testing of Four M06-Class Functionals and 12 Other Functionals. *Theor. Chem. Acc.* **2008**, *120*, 215–241. <https://doi.org/10.1007/s00214-007-0310-x>.
- (44) Dreuw, A.; Head-Gordon, M. Single-Reference Ab Initio Methods for the Calculation of Excited States of Large Molecules. *Chem. Rev.* **2005**, *105*, 4009–4037. <https://doi.org/10.1021/cr0505627>.
- (45) Provorov Long, M. R.; Isborn, C. M. Combining Explicit Quantum Solvent with a Polarizable Continuum Model. *J. Phys. Chem. B* **2017**, *121*, 10105–10117. <https://doi.org/10.1021/acs.jpcc.7b06693>.